The Impact of Tropical Atlantic Freshwater Fluxes on the North Atlantic Meridional Overturning Circulation

by

John Paul Gordon Spence

B.Sc., University of Victoria, 2000

A Thesis Submitted in Partial Fulfillment of the
Requirements for the Degree of

Master of Science

in the School of Earth and Ocean Sciences

Supervisor: Dr. Andrew. J. Weaver

Abstract

The influence of ENSO-related changes in the Atlantic-to-Pacific freshwater budget on the North Atlantic meridional overturning is examined using the UVic Earth System Climate Model. The initial analysis of freshwater fluxes in the NCEP50 reanalysis product and GPCP data set reveals that the transport of water vapour out of the tropical Atlantic drainage basin is enhanced during El Niño phases and reduced during La Niña phases; a one standard deviation in the southern oscillation index alters the tropical Atlantic freshwater balance by about 0.09 Sv. A weaker link with ENSO is found in the ERA40 reanalysis although its usefulness is severely limited by a strong, and spurious, trend in tropical precipitation. Model results suggest that tropical Atlantic salinity anomalies generated with the frequency and amplitude of ENSO tend not to impact deep water formation as they are diluted en route to the North Atlantic. Lower frequency, decadal timescale anomalies, however, do have an impact, albeit weak, on the rate of North Atlantic Deep Water formation. In addition, and contrary to earlier results, it is found that even a shift of the tropical Atlantic freshwater balance towards permanent El Niño conditions only slightly mitigates the transient reduction of North Atlantic Deep Water formation associated with the increase of anthropogenic greenhouse gases. Taken together, the results suggest that the poleward propagation of salinity anomalies from the tropical Atlantic, associated with changes in ENSO, should not be considered a significant mechanism for the variability of the North Atlantic meridional overturning in the present and foreseeable future climate.

Table of Contents

List of Tables

List of Figures

Acknowledgements

I wish to thank my supervisor Andrew Weaver for his guidance and mentorship. I am also grateful to Wanda Lewis, Ed Wiebe, Michael Eby and the rest of the climate lab for providing a wonderful learning environment.

Special thanks to my family for their support and encouragement; my deep gratitude to Roberta and Paul Harris, Michael Burlington (in memory), John, Joan, Holly and Tom Spence, Sean, Lucy, and Elliot Spence, Gordon (in memory) and Alice Stevens, Tom (in memory) and Winnifred Burlington, as well as Jack (in memory) and Norma (in memory) Spence.

This research was supported by the National Science and Engineering Research Council, the Canadian Foundation for Climate and Atmospheric Studies and the Canadian Climate Variability Research Network.

Chapter 1

Introduction

1.1 Study Motivation

The transport of heat from low to high latitudes by the North Atlantic meridional overturning circulation (NAMOC) is widely recognized as a key component of northern hemisphere climate. Ganachaud and Wunsch (2003) estimate the present-day northward heat transport by the NAMOC to be 1.3 PW at 24°N, or roughly 70% of the global ocean meridional heat transport at that latitude. Open ocean deep convective mixing, triggered by extreme surface cooling events during the North Atlantic winter, is an important component of the NAMOC (Marshall and Schott 1999). It establishes the large-scale pressure gradients which allows for the formation of North Atlantic Deep Water (NADW) (Dickson and Brown 1994). Diapycnal mixing is the primary means of warming cold deep waters, allowing them to rise through the thermocline and flow to the North Atlantic via the wind driven surface circulation, completing the NAMOC (Gregg 1989, Polzin et al. 1995). Data based estimates of present-day NADW mass transports in the Atlantic typically range from 15-22 Sv (1 Sv = 1.0×10^6 m^3s^{-1}) (Ganachaud and Wunsch 2000, Talley et al. 2003). Paleoclimate evidence linking variations in the rate of NADW formation with rapid changes in North Atlantic and European climate (Bond et al. 1993, Broecker 1997), combined with model studies demonstrating its sensitivity to surface freshwater fluxes (Stommel 1961, Manabe and Stouffer 1988, Weaver and Hughes 1992), has raised the question of potential impacts of anthropogenic forcing on the NAMOC.

The Intergovernmental Panel on Climate Change Third Assessment Report report (TAR) showed that most climate models project a decrease (roughly 2-10 Sv) in the strength of the NAMOC over this century in response to increased greenhouse gas concentrations (Houghton et al. 2001) (Fig. 1.1). Despite differences in complexity and a wide range of responses, these models show qualitatively similar behaviour; warmer sea surface temperatures and an increase in freshwater input at high latitudes from an enhanced hydrological cycle results in more stably stratified North Atlantic surface waters and reduced NADW formation. An exception discussed in the TAR is

the ECHAM4/OPYC model, which projected a stable NAMOC under global warming conditions. It was argued that in this model the local effects of warming and freshening on the surface density of the North Atlantic were mitigated by the advection of positive salinity anomalies from the the tropical Atlantic (Latif et al. 2000). The salinity anomalies, in turn, were suggested to have been created by a shift in the tropics towards more frequent El Niño conditions, which increased the amount of freshwater exported from the tropical Atlantic (Timmermann et al. 1999). Latif et al. (2000) argued that this feedback is a stronger feature in their model because it had a high meridional resolution of 0.5°N in the tropical oceans, which enabled it to better resolve tropical air-sea interactions. The results of Latif et al. (2000) highlighted the influence of ENSO on the freshwater balance of the tropical Atlantic as a possible important mechanism for NAMOC variability.

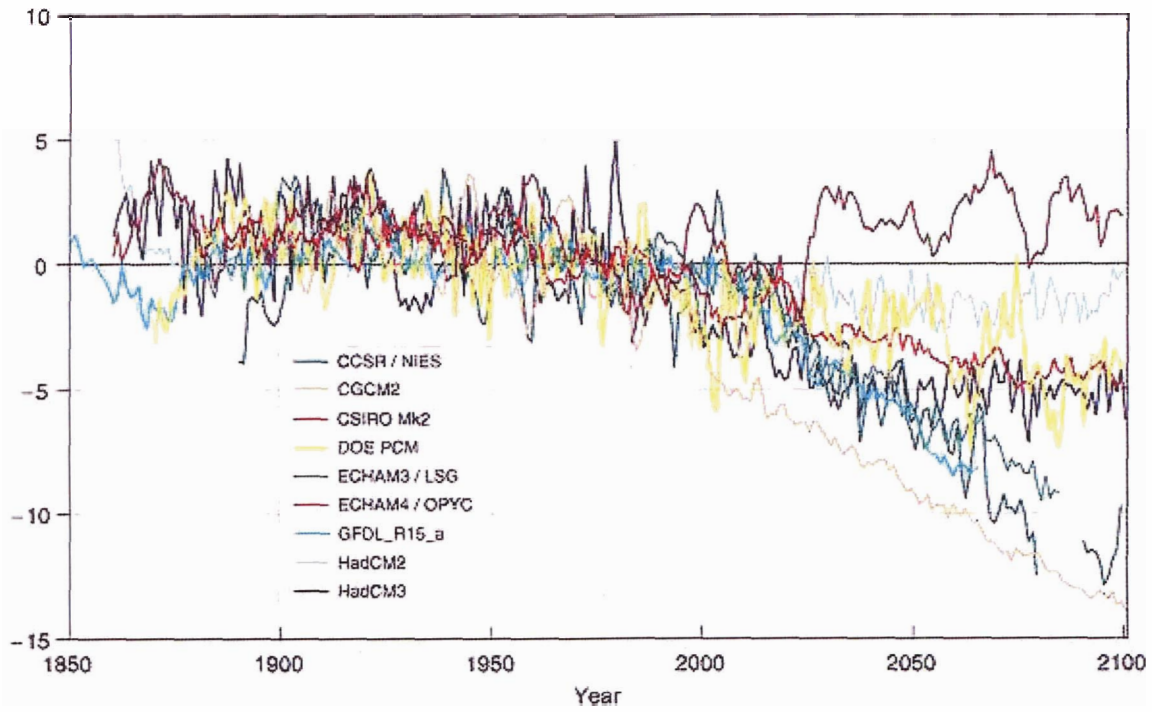

Figure 1.1: **Changes in the strength of the NAMOC (Sv) in coupled climate models published in the TAR (Houghton et al. 2001). Shown is the annual mean relative to the mean of the years (1961 to 1990). The future-forcing scenario is the IS92a emissions scenario.**

The goal of this dissertation is to examine the interannual variability in the tropical Atlantic surface freshwater flux and its impact on the NAMOC. I begin with brief discussions of ENSO and its link to the tropical Atlantic in the following subsections. Then I examine the influence of ENSO on tropical Atlantic freshwater fluxes in Chap-

ter 2. Chapter 3 introduces the climate model and experimental design employed. In Chapter 4, I evaluate the impact of tropical Atlantic freshwater fluxes on an equilibrated climate. I determine if a reasonable increase in tropical Atlantic freshwater export, comparable to present-day El Niño conditions, mitigates the high-latitude effects on NADW formation under anthropogenic warming conditions in Chapter 5. Conclusions are presented in Chapter 6.

1.2 Overview of ENSO

ENSO is regarded as the strongest interannual variation in climate (Houghton et al. 2001). It originates in the tropical Pacific through coupled interactions between the ocean and atmosphere, which generate anomalous sea surface temperature (SST) and sea level pressure (SLP) conditions (see Neelin et al. (1998) for a comprehensive review of ENSO). Canonical El Niño events are characterized by positive SST anomalies in the eastern equatorial Pacific that weaken the normally strong zonal gradient. In turn, the zonal SLP gradient is reduced and the Pacific trade winds are weakened. The weakening of the trade winds leads to a reduction in the upwelling of cold water on the eastern coast of the Pacific and an eastward shift in the warm surface water from the western tropical Pacific, both of which act to enhance the initial increase in SST and shoal the thermocline. Correspondingly, the large-scale convective precipitation that is typically found in the western tropical Pacific follows the warm surface water eastward. The weakened trade winds also cause off-equatorial thermocline depth anomalies that propagate westward as weak upwelling Rossby waves. When Rossby waves reach Indonesia they are reflected and propagate eastward as upwelling Kelvin waves. When the Kelvin waves reach the central-eastern Pacific, where the thermocline is close to the surface, their upwelling influence can be strong enough to change the sign of the SST anomalies and lead to La Niña conditions. Canonical La Niña events can be characterized as an enhancement of the tropical Pacific mean state. Both the zonal SST and SLP gradients are strengthened.

The ENSO cycle has demonstrated considerable spatial, temporal and amplitudinal variability over the modern record (Houghton et al. 2001). This variability is often attributed to stochastic forcing due to atmospheric weather noise (Burgers 1999) and deterministic chaos arising from the nonlinear interaction of ENSO with the seasonal cycle (Jin et al. 1994, Tziperman et al. 1994). However, the work of Trenberth and Hoar (1996) has received considerable attention for postulating a link between an apparent shift in observed ENSO activity with anthropogenic climate change. They

argued that the tendency for more frequent, persistent and intense El Niño events since the late 1970's is highly unusual and unlikely to be accounted for solely by natural variability. The statistical significance of their results has been challenged (Harrison and Larkin 1997, Wunsch 1999). Some modelling results (Knutson and Manabe 1998, Timmermann et al. 1999) have corroborated the findings of Trenberth and Hoar (1996), but are suspect in view of their inability to fully simulate ENSO and the strong natural variability observed (Houghton et al. 2001).

1.3 The Atmospheric Bridge: Linking ENSO to the Tropical Atlantic

The link between ENSO and the tropical Atlantic is part of the 'atmospheric bridge' identified by Lau and Nath (1994). Changes in the precipitation patterns of the tropical Pacific and the associated release of latent heat during ENSO events force large-scale atmospheric waves. These waves can alter the temperature, humidity, wind and distribution of clouds far from the equatorial Pacific and result in changes in surface heat, freshwater and momentum fluxes (Alexander et al. 2002). Through this 'atmospheric bridge' it is possible for the influence of ENSO events to 'teleconnect' around the globe.

ENSO's link to the tropical Atlantic was first documented by Covey and Hastenrath (1978). Using composites of SST, SLP and winds in the tropical Atlantic, they identified an increase (decrease) in SST in a broad region just north of the equator roughly 3-6 months after El Niño (La Niña) events. Subsequent observational analyses (Curtis and Hastenrath 1995, Enfield and Mayer 1997) confirmed the results of Covey and Hastenrath (1978), and have further identified a reduction in sea level pressure, a weakening of the northeast trade winds, and a northward shift in the Intertropical Convergence Zone (ITCZ) following El Niño events. The inverse of this pattern of response generally holds for La Niña events.

It is well established that more water is exported from the tropical Atlantic than imported (Baumgartner and Reichel 1975). Of particular importance to this study is identifying how ENSO related variability impacts the negative surface freshwater balance of the Atlantic. Schmittner et al. (2000) examined the influence of ENSO on tropical Atlantic freshwater export in a 39 year (1958 to 1996) National Centers for Environmental Prediction (NCEP) reanalysis (NCEP40) (Kalnay et al. 1996), and a 15 year (1979 to 1993) European Centre for Medium-Range Weather Forecasts

(ECMWF) reanalysis (ERA15) (Gibson et al. 1997). They found that freshwater export out of the tropical Atlantic is enhanced during El Niño events and is reduced during La Niña events by approximately 0.05-0.2 Sv (depending on the strength of the event). Using a simple, zonally averaged climate model Schmittner et al. (2000) also found that permanent shifts in tropical Atlantic freshwater export in this range affected the NAMOC.

Chapter 2

The Influence of ENSO on Tropical Atlantic Freshwater Fluxes

2.1 Estimates of Surface Freshwater Fluxes Used in this Study

Since Schmittner et al. (2000), NCEP has expanded its reanalysis to 57 years spanning 1948 to 2005 (NCEP50) (Kistler et al. 2001), and ECMWF released a new 45 year reanalysis (ERA40) spanning 1957 to 2002 (Kållberg et al. 2004). In this chapter I follow Schmittner et al. (2000) and re-examine the influence of ENSO on the surface freshwater balance of the tropical Atlantic drainage basin in NCEP50 and ERA40. It is important to recognize that precipitation (P) and evapouration (E) in these products are completely determined by the reanalysis model; no direct observations are used. The models estimate P and E at consistent spatial and temporal scales by combining observations of the state of the atmosphere with short term model forecasts. Since results determined from reanalysis products should be compared with independent observational estimates, I also examine the Global Precipitation Climatology Project data set (GPCP) (Huffman et al. 1997).

I calculate surface freshwater anomalies in NCEP50 and ERA40 from monthly mean P-E fluxes at $1.9°\times1.9°$ and $2.5°\times2.5°$ horizontal resolution, respectively. In both models, convective and large-scale condensation and the surface latent flux are generated by short term model forecasts and output every six hours. E is calculated by dividing the surface latent heat flux by the latent heat of vapourization of water. P is calculated by summing the total amount of convective and large-scale precipitation that reaches the surface. Surface P-E fluxes in NCEP50 and ERA40 are not strictly conserved over the globe. Conservation can be achieved by subtracting the global surface P-E imbalance for each month so that the area weighted sum becomes zero. I found that the differences between globally conserved and unconserved fluxes were inconsequential and the analysis presented in this dissertation is based on the unconserved fluxes.

The GPCP data set was created by merging rain gauge measurements and satellite estimates of P. The merging procedure is designed to incorporate data based on an estimate of its quality, with an emphasis given to rain gauge measurements. I calculate freshwater anomalies in GPCP from monthly mean P fluxes at $2.5° \times 2.5°$ resolution. Since precipitation is not directly assimilated into the reanalysis models, a comparison to GPCP provides an independent measure of their performance.

2.2 The Southern Oscillation Index of ENSO

The Southern Oscillation Index (SOI) is a measure of the large-scale fluctuations in air pressure between the western and eastern tropical Pacific that are characteristic of ENSO events. It is traditionally calculated from differences in SLP anomalies between Papeete, Tahiti and Darwin, Australia. The advantage of using the SOI as an index of ENSO rather than indices based on fluctuations in SST across the tropical Pacific is that it can be calculated directly from the NCEP50 and ERA40 reanalysis products; the reanalysis models do not output SST. Calculating the SOI directly from the reanalysis products allows a comparison to observations to get a first order approximation of how well the reanalysis models capture the atmospheric component of ENSO. When smoothed, the SOI generally corresponds very well with SST based indices of ENSO (Wallace et al. 1998).

The observational SOI provided by the National Oceanic and Atmospheric Association (NOAA) is used to evaluate the reanalysis models (NOAA 2005a). The SOI is calculated from NCEP50 and ERA40 in the manner outlined by NOAA (NOAA 2005b). First, standardized time series of Tahiti and Darwin SLP anomalies are calculated as follows:

$$Standardized\ Tahiti = \frac{SLP\ Tahiti - mean(SLP\ Tahiti)}{\sqrt{\frac{\sum_{i=1}^{N}(SLP\ Tahiti(i) - mean(SLP\ Tahiti))^2}{N}}}, \tag{2.1}$$

$$Standardized\ Darwin = \frac{SLP\ Darwin - mean(SLP\ Darwin)}{\sqrt{\frac{\sum_{i=1}^{N}(SLP\ Darwin(i) - mean(SLP\ Darwin))^2}{N}}}. \tag{2.2}$$

Mean SLP values are determined from the 1951-1980 base period for NCEP50, as recommended by NOAA. The ERA40 mean is determined from the 1958-1980 base period. N is the number of months of data. The SOI is calculated from the standard-

ized anomalies as

$$SOI = \frac{Standardized\ Tahiti - Standardized\ Darwin}{\sqrt{\frac{\sum_{i=1}^{N}(Standardized\ Tahiti(i) - Standardized\ Darwin(i))^2}{N}}} \tag{2.3}$$

Figure 2.1 shows the NOAA SOI and the SOI calculated from reanalysis models (in units of standard deviations (SD)). A sliding 12 month low pass filter (refer to Appendix A for details) was applied to smooth the time series. There is very little difference between the three time series, which is indicative of the reanalysis models being strongly influenced by observations of atmospheric pressure. Sustained negative (positive) values of the SOI typify the characteristic weakening (strengthening) of zonal tropical Pacific surface winds during El Niño (La Niña) events. Power spectra of the SOI show a preferred four year period over the last 50 years, although in the historical record the period has varied between two and seven years (Neelin et al. 1998). The similarity of the time series in Fig. 2.1 permits the use of the NOAA SOI as a common index of ENSO in the analysis of tropical Atlantic freshwater fluxes from NCEP50, ERA40 and GPCP in sections 2.3 and 2.4.

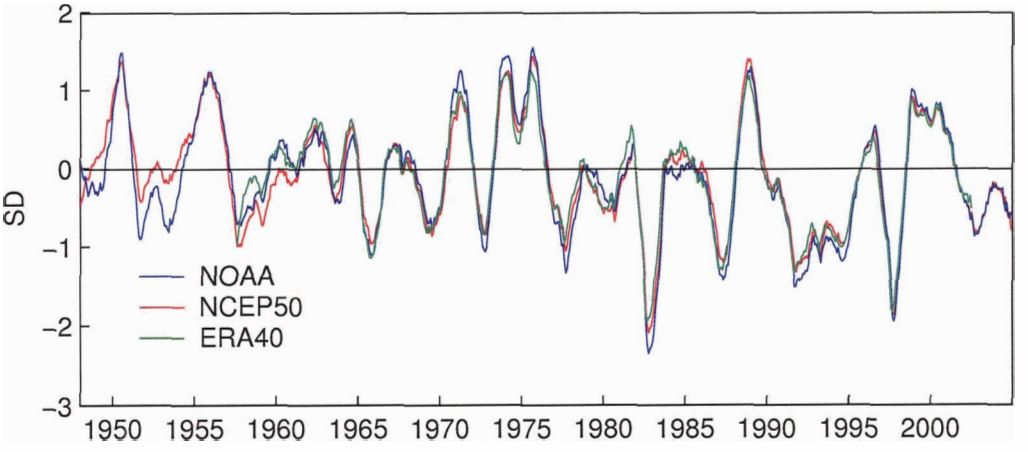

Figure 2.1: **Time series of the SOI from NOAA, NCEP50 and ERA40.**

2.3 Integrated Anomalous Freshwater Flux Time Series and the SOI

Figure 2.2 shows the times series of freshwater anomalies (when they are integrated over the Atlantic drainage basin between 20°S and 20°N) for the three data sets, along with the NOAA SOI. A clear correlation between the SOI and anomalies from

GPCP and NCEP50 can be seen. Decreases (increases) in the SOI, tending towards El Niño (La Niña) conditions, are correlated with decreases (increases) in freshwater anomalies. The figure also reveals the erroneous trend in ERA40 anomalies, which is caused by a strong trend in tropical P in the later years of the reanalysis. ECMWF have identified the problem as stemming from errors in the analysis of humidity from satellite observations (Troccoli and Kallberg 2004). Inadequate bias corrections were applied and the effect of aerosols released by the eruption of Mount Pinatubo in 1991 were not properly accounted for. The similarity between the NCEP50 and GPCP regressions indicates that the variability is largely driven by anomalous P.

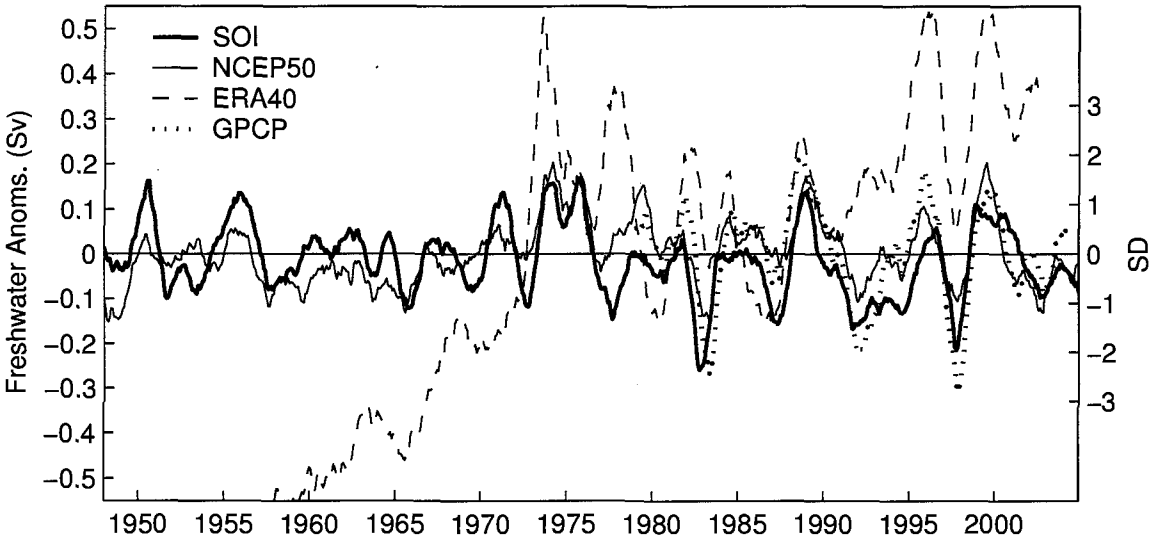

Figure 2.2: **Time series of the SOI (right axis) with NCEP50 and ERA40 surface P-E anomalies, and surface P anomalies from GPCP. The monthly anomalies were smoothed with a sliding 12 month low pass filter (Appendix A) and integrated over the tropical Atlantic drainage basin from 20°S to 20°N. The zonal bounds of the drainage basin are shown in Fig. 2.3.**

Table 2.1 shows the results of a linear regression of the SOI with the freshwater time series from Fig. 2.2. Details of the linear regression algorithm are provided in Appendix B. The correlations and slopes of the regression lines from ERA40 show a weak and highly uncertain correlation with ENSO. In an attempt to reduce the effect of the strong P trend in ERA40 I detrended the time series. The detrended ERA40 time series correlation improved marginally, but is still poor in comparison to the other data sets. Results from NCEP50 show a weaker link to ENSO than found with GPCP. Kistler et al. (2001) note the introduction of satellite data in 1979 dramatically improved the quality of the reanalysis. I follow their strong recommendation and evaluate NCEP50 anomalies separately for the satellite era, denoted NCEP50_SAT.

Table 2.1: **Results of linearly regressing the SOI with integrated tropical Atlantic freshwater anomalies**

Freshwater Data Source	SOI Correlation	SOI Regression Slope (Sv/SD)
ERA40 P-E 1957/09–2002/08	0.08 ±0.08	0.033 ±0.034
ERA40 P-E 1957/09–2002/08 detrended	0.34 ±0.08	0.081 ±0.02
NCEP50 P-E 1948/01–2004/12	0.59 ±0.05	0.065 ±0.006
NCEP50_SAT P-E 1979/01–2004/12	0.79 ±0.04	0.087 ±0.007
GPCP P 1979/01–2004/09	0.75 ±0.05	0.10 ±0.01

Correlation coefficients, regression slopes and confidence intervals were determined by linearly regressing surface freshwater anomalies integrated over the Atlantic drainage basin between 20°S and 20°N with the SOI. The confidence intervals were calculated without accounting for autocorrelation. The timeseries are shown in Figure 2.2, except for the NCEP50_SAT and the detrended ERA40.

The NCEP50_SAT integrated time series nearly overlies the full-length one and is plotted independently in Fig. 3.1. Differences between the two NCEP50 series result from the different time periods used to calculate the longterm monthly means. Regression results with NCEP50_SAT anomalies compare well with GPCP and show a slightly stronger link between ENSO and tropical Atlantic freshwater fluxes than was found by Schmittner et al. (2000). They found SOI correlations of 0.65 and 0.68, and slopes of 0.06 and 0.08 for NCEP40 and ERA15, respectively. The average total freshwater export in the Atlantic drainage basin between 20°S and 20°N determined from NCEP50_SAT is 0.23 Sv. A one SD decrease in the SOI increases this export by roughly 35% to 45% according to the regression analysis.

The only other significant correlation I found between ENSO and Atlantic freshwater fluxes was between 20°N and 40°N. When freshwater anomalies are integrated over this region, the NCEP50_SAT correlation with the SOI is -0.37 ±0.06 and the regression slope is -0.018 ±0.04. For GPCP, the correlation is -0.55 ±0.08 and the slope is -0.021 ±0.04. This is consistent with an extratropical link between ENSO and the Pacific-North American pattern (Giannini et al. 2001). Following El Niño events, this teleconnection results in increased P in the extratropics, especially over the southeastern United States, and is essentially a weaker and anticorrelated version of ENSO's impact on the tropical Atlantic freshwater flux.

2.4 Spatial Pattern of the Influence of ENSO on Tropical Atlantic Freshwater Fluxes

I identify the spatial pattern of the influence of ENSO on surface freshwater fluxes in the tropical Atlantic drainage basin by linearly regressing NCEP50, NCEP50_SAT and GPCP P anomalies with the SOI at each grid point (Fig. 2.3). The spatial pattern and magnitudes in all three regressions are similar with the dominance of positive signals indicating increased freshwater export under El Niño conditions. In general, they show a strong positive signal along the northeast coast of South America, and weaker positive signals across the equatorial Atlantic and in the southeastern Sahel region of Africa. Negative signals are found in the northern Caribbean, the Parana-Plata basin (central Brazil) and around Lake Victoria, Africa. These results are consistent with the observed ENSO-related rainfall patterns of Giannini et al. (2000) and Rao et al. (1993) in Central and South America, of Ropelewski and Halpert (1987) and Janicot et al. (2001) in Africa, and with studies of the tropical Atlantic freshwater budget by Saravanan and Chang (2000) and Yoo and Carton (1990).

The spatial pattern from the full-length NCEP50 regression compares very well with the picture presented by Schmittner et al. (2000) from their regression of NCEP40 with the SOI. Both show a more prominent signal in the south-central Sahel region and the Parana-Plata basin, as well as a less prominent signal in the Amazon basin and across tropical Atlantic Ocean, than is present in the satellite era NCEP50 and GPCP regressions. The negative signal around Lake Victoria, Africa in the NCEP50_SAT regression is of note because it is stronger and shifted westward in comparison to the others, giving it a greater impact on the tropical Atlantic drainage basin.

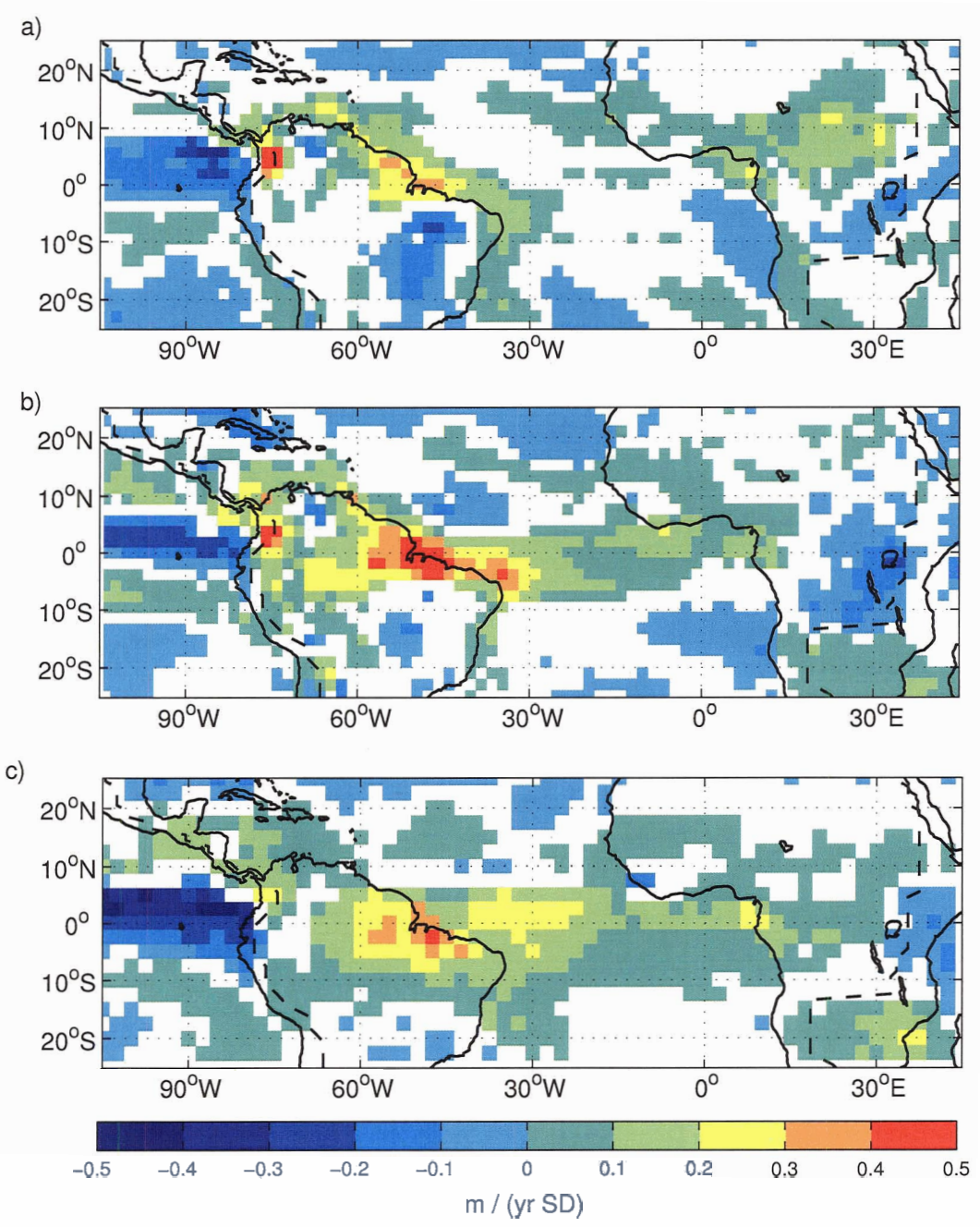

Figure 2.3: Shown is the change in surface freshwater flux anomalies due to an increase in the SOI by one SD. Frame (a) uses NCEP50 P-E anomalies, (b) uses NCEP50_SAT P-E anomalies and (c) uses GPCP P anomalies. The freshwater anomalies are linearly regressed with the SOI at each grid point (Appendix B). The slope of the regression line is plotted if its correlation coefficient exceeds the 95% confidence interval. Monthly anomalies are smoothed prior to regression (Appendix A). Confidence intervals were calculated without accounting for autocorrelation. The zonal boundary of the tropical Atlantic drainage basin, indicated by the black dashed line, was provided by A. Schmittner and was used in Schmittner et al. (2000).

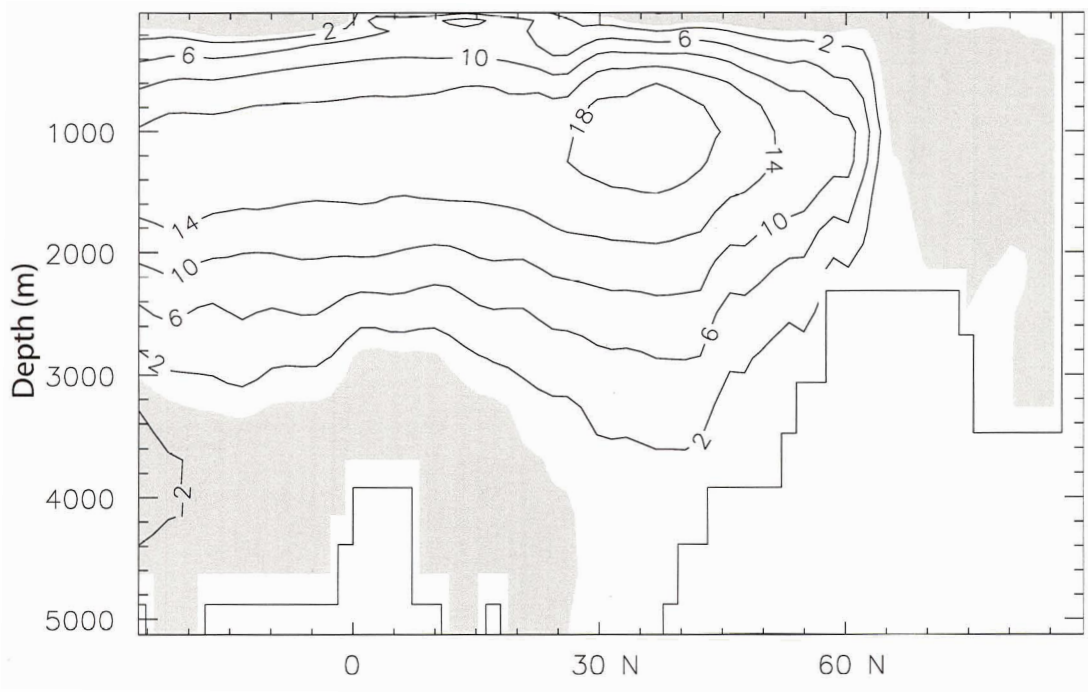

Figure 4.1: **Annual mean meridional overturning stream function (Sv) for the North Atlantic in year 4500 of CNTRL. Shaded regions are negative.**

4.2 Response to Constant Forcing

As discussed in section 2, strong ENSO events correspond to changes in tropical Atlantic freshwater export in the range of 0.1-0.2 Sv. Using a zonally-averaged model, Schmittner et al. (2000) found that adding freshwater to the tropical Atlantic at a rate of 0.2 Sv, corresponding to a strong La Niña event, for 70 years led to a collapse of the NAMOC. Under El Niño conditions of the same magnitude their NAMOC re-equilibrated about 20% stronger after 70 years. Here I evaluate the generality of their results by examining the response of the NAMOC in the more sophisticated UVic ESCM to permanent shifts in the tropical Atlantic freshwater balance.

The freshwater forcings are applied in the spatial pattern of the NCEP50_SAT regression (Fig. 2.3b) to simulate shifts towards El Niño and La Niña conditions. Because of this, the magnitude of the forcings are in units of SD of the SOI. A 1 SD decrease is equivalent to increasing the freshwater export of the tropical Atlantic by 0.073 Sv when integrated over the forcing pattern. This is less than indicated in

capture the gross pattern of ENSO's influence on the tropical Atlantic freshwater flux, they fail to capture irregularities in the tropical Atlantic response.

Chapter 3

Model Description and Experimental Design

3.1 The University of Victoria Earth System Climate Model

This study uses version 2.7 of the intermediate complexity University of Victoria Earth System Climate Model (UVic ESCM). The UVic ESCM couples a 3-D ocean general circulation model, a 2-D atmospheric model, a thermodynamic/dynamic sea ice model, and a land surface model. It is described in detail in Weaver et al. (2001). All components have a zonal resolution of 3.6° and a meridional resolution of 1.8°. The UVic ESCM is forced from start-up to equilibrium by variations in insolation and surface winds. Heat and freshwater are conserved to machine precision without the use of flux adjustments.

The ocean component is version 2.2 of the Geophysical Fluid Dynamics Laboratory Modular Ocean Model (Pacanowski 1995). It has 19 vertical levels that increase parabolically in thickness from 50m at the surface to 518m at depth. The isopycnal and horizontal viscosity coefficients are set at 4.0×10^{2} m^2s^{-1} and 2.0×10^{5} m^2s^{-1}, respectively. The vertical diffusivity ranges from 3.0×10^{-5} m^2s^{-1} at the surface to 1.3×10^{-4} m^2s^{-1} at depth according to the scheme of Bryan and Lewis (1979). Mixing associated with mesoscale eddies is parameterized according to Gent and McWilliams (1990). The ocean model uses a constant salt-to-freshwater mass ratio of 3.49×10^{-2} to convert surface freshwater fluxes to fluxes of salt.

The UVic ESCM employs a vertically integrated energy-moisture balance atmospheric model for computational efficiency. The underlying philosophy being that on time scales greater than a decade the ocean is a key prognostic component of the climate system (Weaver 2004). Momentum conservation equations are replaced by specified wind fields and the thermodynamic energy balance equations are vertically integrated. This leaves a single atmospheric layer that captures the climatic mean state in the absence of atmospheric variability. Radiative forcing associated with

changes in atmospheric CO_2 is included as a change in the outgoing longwave radiation. P in the form of rain or snow occurs when the relative humidity exceeds 85%. Surface winds are prescribed from the longterm monthly mean climatology of the NCEP50 reanalysis (Kistler et al. 2001). The UVic ESCM does not simulate ENSO because their is no interannual variability in the winds due to the lack of explicit atmospheric dynamics.

P on land is treated by a simple bucket model, detailed by Matthews et al. (2003). Inputs to the bucket are rain and snowmelt; outputs are E and river runoff. Runoff occurs when a grid cell's 15 cm deep bucket overflows, and it is returned to the ocean via weighted river discharge points. The parameterization of E on land includes a surface resistance. Surface resistance decreases as a bucket fills and is dependent on vegetation type. One of seven vegetation types are statically assigned to each grid cell. The vegetation type also determines the land surface albedo in the absence of snow.

The sea ice model incorporates energy conserving ice-snow thermodynamics with a 2-category thickness distribution (Bitz et al. 2001), and an elastic-viscous-plastic rheology (Hunke and Dukowicz 1997). The model predicts ice thickness, areal fraction and surface temperature.

The UVic ESCM has been used to investigate many scientific questions in both contemporary and paleoclimates. The model was thoroughly validated against present-day climatology in Weaver et al. (2001) and various proxy paleo-reconstructions in Schmittner et al. (2002), Meissner et al. (2003) and Cottet-Puinel et al. (2004). Its computational efficiency and ability to maintain a stable climate without explicit flux adjustments permits a wide range of parameter sensitivity studies over long timescales (e.g. Wiebe and Weaver (1999), Lewis et al. (2003), Hickey and Weaver (2004)).

3.2 Experimental Design

I investigate the influence of tropical Atlantic freshwater fluxes on the NAMOC by conducting a series of freshwater sensitivity studies initialized from an equilibrium pre-industrial climate. Surface freshwater fluxes are always applied to the tropical Atlantic drainage basin between 20°S and 20°N in model year 4500. Over land, the fluxes are applied directly to river runoffs and in the ocean they are treated as fluxes of salt. The tropical Atlantic drainage basin in the UVic ESCM does not exactly correspond to the drainage basin shown in Fig. 2.3 because the model has a coarser resolution. Salt is conserved in the experiments by spreading an equivalent opposing

surface flux over the tropical Pacific. I decided to focus the model results presented in this dissertation on NCEP50 anomalies rather than GPCP because NCEP50 covers a longer time span and freshwater fluxes are best analyzed by including the effects of both P and E. Because I am interested in variability at interannual time scales and longer, a sliding 12 month low pass filter is applied to the reanalysis anomalies (Appendix A).

I begin with a series of freshwater sensitivity studies wherein the atmospheric CO_2 concentration is held fixed at a pre-industrial level of 280 ppm. First I evaluate the pre-industrial equilibrium NAMOC in Section 4.1; then I gauge its sensitivity to shifts in the tropical Atlantic freshwater balance towards permanent El Niño and La Niña conditions in Section 4.2. In Section 4.3 sinusoidal freshwater signals of various periods are applied to determine the frequency of variability at which NADW formation is influenced. I examine the impact of NCEP50 P-E anomalies by applying them at each grid point in the forcing region in Section 4.4.

Chapter 5 evaluates the extent to which a shift in tropical Atlantic freshwater export towards El Niño conditions mitigates the weakening of the NAMOC under anthropogenic warming conditions. Section 5.1 begins by examining the NAMOC response to an exponential increase in the concentration of atmospheric CO_2 to 750 ppm over 250 years. I then evaluate the impact of increasing the frequency of El Niño related tropical Atlantic freshwater fluxes. In order to simulate an increase in the frequency of El Niño events I identify ENSO events which had a strong impact on the tropical Atlantic from the integrated NCEP50_SAT P-E anomaly time series (Fig. 3.1). Four time series are generated, each being 250 years long, by concatenating ENSO event anomalies from the gridded NCEP50_SAT data. Zeros are used as padding between the last month of one event and the first month of the next. The first series is created with 50% El Niño events and 50% La Niña events. In choosing a particular event, I chronologically cycle through the four El Niño events and three La Niña events identified in Fig. 3.1. For the second, third and fourth time series I increase the number of El Niño events relative to La Niña events to 66%, 88% and 100%, respectively. I then run model experiments with the same exponential increase in CO_2 and with each time series dictating the tropical Atlantic freshwater forcing. In a similar fashion, I evaluate the effect of increasing anomaly amplitudes during El Niño events in Section 5.2. Three more time series are generated, only this time the number of El Niño events relative to La Niña events is held fixed at 50%, and the amplitude of El Niño event anomalies are increased by 25%, 50% and 100%.

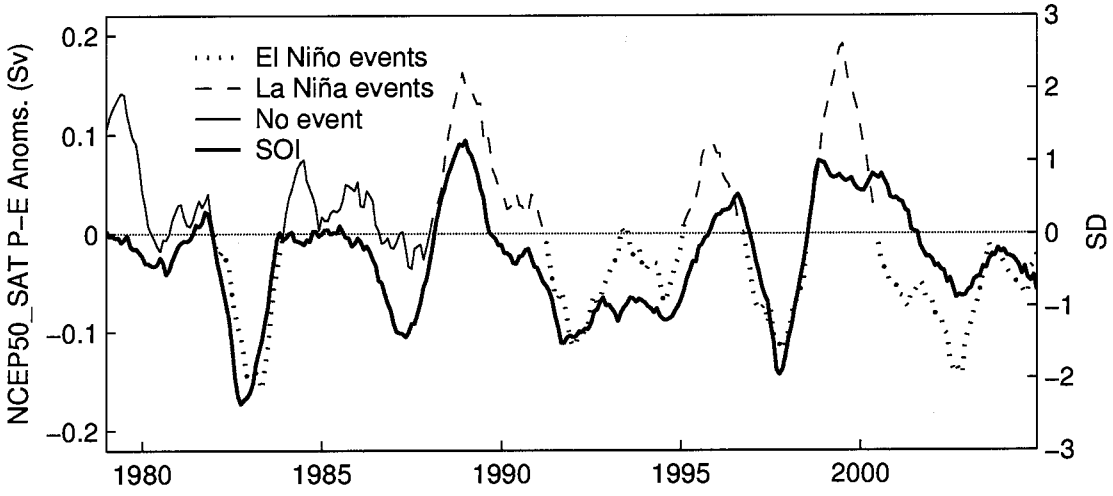

Figure 3.1: Time series of the SOI (right axis) and NCEP50 P-E anomalies determined solely from the satellite era (1979/01 to 2004/12) in the same manner as the series in Fig. 2.2. The marked El Niño events of 1983, 1992, 1998 and 2001 along with the La Niña events of 1989, 1995 and 1999 are used to generate freshwater forcing timeseries with an increased frequency and amplitude of El Niño events.

Chapter 4

NAMOC Response to Tropical Atlantic Freshwater Forcing with CO_2 Fixed

4.1 The Pre-industrial NAMOC

The equilibrated model run, denoted CNTRL, is achieved by integrating the UVic ESCM for 4500 years with an atmospheric CO_2 concentration of 280 ppm (equivalent to the concentration in the year 1850). Figure 4.1 shows the equilibrated transport of water by the NAMOC in CNTRL. The NAMOC transport in the model is depicted by the stream function of the zonally-integrated volume transport:

$$\Phi(\phi, z) = \int_z^0 \int_{\lambda_W}^{\lambda_E} a\, cos\phi\, v(\lambda, \phi, z')\, d\lambda\, dz'. \tag{4.1}$$

The meridional velocity, v, is integrated over depth and from the western (λ_W) to the eastern boundary (λ_E) of the North Atlantic ocean domain; a denotes the radius of the Earth. Figure 4.1 shows that roughly 20 Sv of NADW formation occurs although it has a tendency to form too far south (Weaver et al. 2001), while 2.5 Sv of Antarctic bottom water extends to about 20°N and fills the North Atlantic up to a depth of about 3000 m.

The principal means I use to detect changes in NADW formation is to examine changes in the maximum value of the NAMOC transport between the latitudinal bounds of 26°N and 70°N, and depths of 170 m and 4000 m (NAMOC strength hereafter). CNTRL produces a reasonable equilibrium NAMOC strength of 20.5 Sv with some internal weak variability which has a dominant period of roughly 25 years. The source of the internal variability is linked to freshwater and heat fluxes resulting from sea ice edge variability.

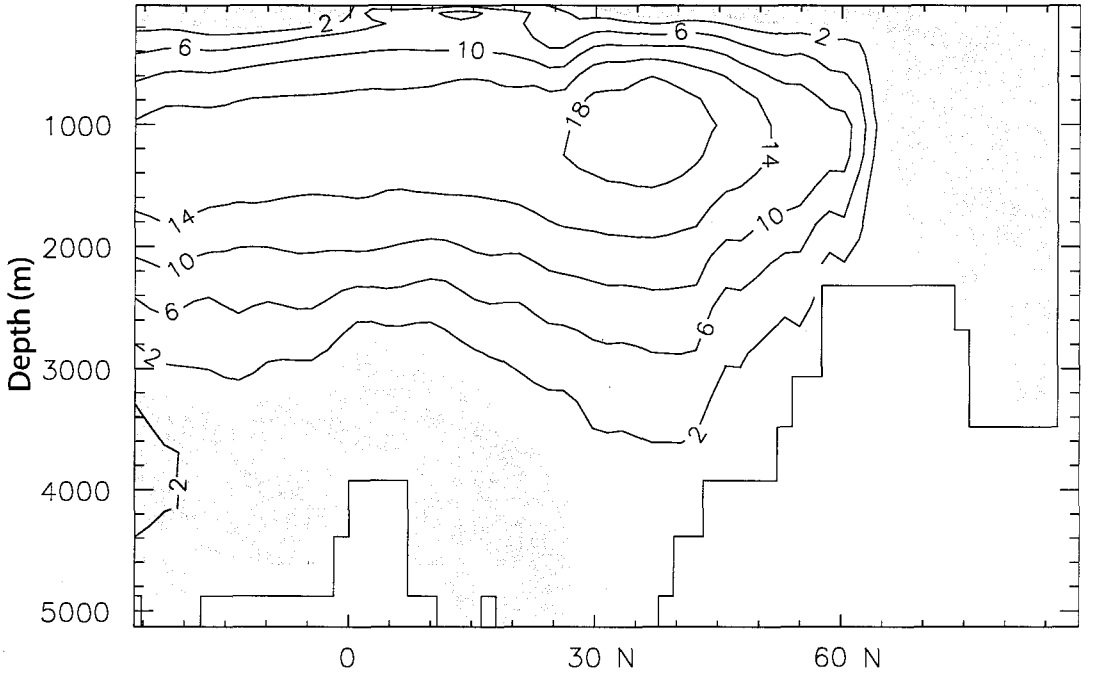

Figure 4.1: **Annual mean meridional overturning stream function (Sv) for the North Atlantic in year 4500 of CNTRL. Shaded regions are negative.**

4.2 Response to Constant Forcing

As discussed in section 2, strong ENSO events correspond to changes in tropical Atlantic freshwater export in the range of 0.1-0.2 Sv. Using a zonally-averaged model, Schmittner et al. (2000) found that adding freshwater to the tropical Atlantic at a rate of 0.2 Sv, corresponding to a strong La Niña event, for 70 years led to a collapse of the NAMOC. Under El Niño conditions of the same magnitude their NAMOC re-equilibrated about 20% stronger after 70 years. Here I evaluate the generality of their results by examining the response of the NAMOC in the more sophisticated UVic ESCM to permanent shifts in the tropical Atlantic freshwater balance.

The freshwater forcings are applied in the spatial pattern of the NCEP50_SAT regression (Fig. 2.3b) to simulate shifts towards El Niño and La Niña conditions. Because of this, the magnitude of the forcings are in units of SD of the SOI. A 1 SD decrease is equivalent to increasing the freshwater export of the tropical Atlantic by 0.073 Sv when integrated over the forcing pattern. This is less than indicated in

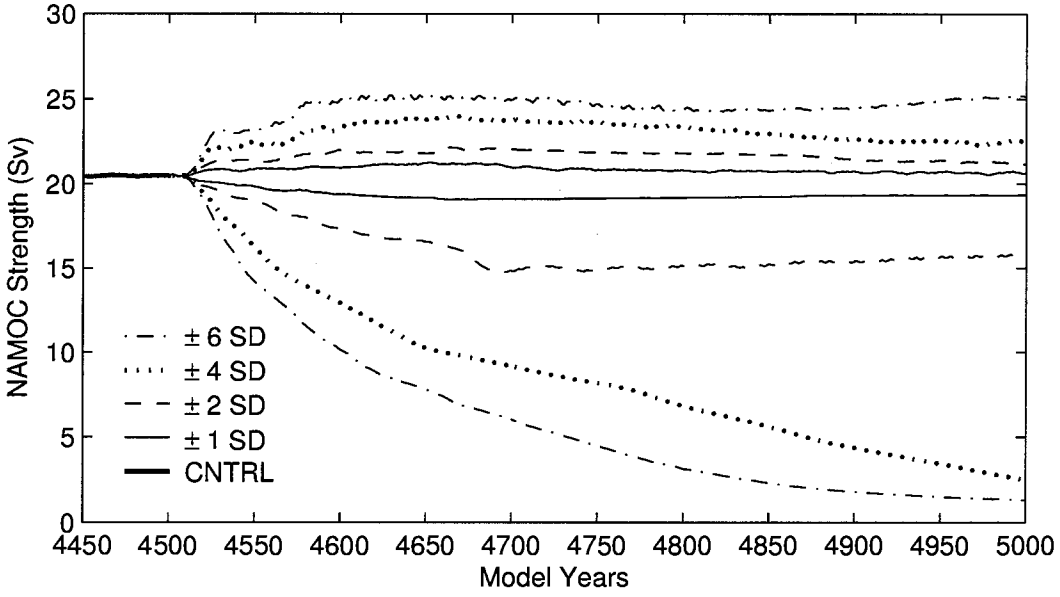

Figure 4.2: **Response of the NAMOC to a range of constant tropical Atlantic freshwater forcings distributed in the spatial pattern of Fig. 2.3b. Negative forcings correspond to El Niño conditions and strengthen the NAMOC. Positive forcings correspond to La Niña conditions and weaken the NAMOC.**

Table 2.1 because it excludes regression values outside the 95% confidence intervals.

Figure 4.2 shows the response of the NAMOC in the UVic ESCM to a range of constant forcings. Changes in the NAMOC begin once the tropical salinity anomalies are advected to the North Atlantic via the Gulf Stream. A 12 year advection time scale was confirmed by passive tracers released at the mouth of the Amazon. The strength of the NAMOC increases (decreases) under El Niño (La Niña) conditions, as expected. The NAMOC response is observed to coincide with changes in the depth of convection in NADW formation regions.

Similar to Schmittner et al. (2000), I find the NAMOC to be more sensitive to salinity decreases than increases. For a permanent disturbance equivalent to a strong present-day El Niño event (~2 SD) the NAMOC strengthens by only 5%. Under La Niña conditions of the same magnitude the NAMOC is weakened by 25% after 500 years. This is due to the sensitive nature of open ocean convection; while increases in surface salinity in convection regions encourages deep water formation, decreases in salinity can actually prevent it (Weaver and Hughes 1992). The modelled convection depth in the North Atlantic stabilizes much more quickly under El Niño forcing conditions than La Niña. After 500 years of -4 SD forcing, equivalent to La Nina conditions twice as strong as observed, the NAMOC approaches a complete collapse.

Overall, I find the NAMOC to be more robust in the model than in Schmittner et al. (2000), which is to be expected in light of the fact that convection and water mass sinking are coupled together (there is no horizontal structure) in zonally-averaged ocean models. Extreme shifts in the tropical Atlantic freshwater balance are required to substantially perturb the NAMOC in the UVic ESCM.

4.3 Response to Sinusoidal Forcing

The goal in applying sinusoidal forcings is to determine if changes in the tropical Atlantic freshwater balance at the frequency and amplitude of ENSO-related variability impacts NADW formation, and if not, then to determine the frequency at which they do. The freshwater forcings are again applied in the spatial pattern of the NCEP50_SAT regression (Fig. 2.3b).

Figure 4.3 shows the NAMOC response to sinusoidal forcings with an amplitude of 2 SD of the SOI, and periods of 7, 14 and 21 years. Considering the 7 year period forcing, I find that while the NAMOC response is oddly offset from the other forcing signals, and the internal variability of the NAMOC is disturbed, the overall impact on the NAMOC is weak (less than 0.1 Sv). Figure 4.4a presents a Hovmoeller diagram of the poleward propagation of salinity anomalies for this forcing. It shows the salinity anomalies to be quickly diluted on their way to the North Atlantic with little impact outside of the forcing region. A distinct sinusoidal NAMOC response is observed for the 21 year period forcing, with the NAMOC responding at a similar frequency to the forcing. Figure 4.4b shows salinity anomalies at this frequency to be entrained in the subtropical gyre, and persisting en route to the North Atlantic. The model response to the 14 year period forcing is comparable to the 7 year signal in this experiment, except for the offset from the 7 year period NAMOC response.

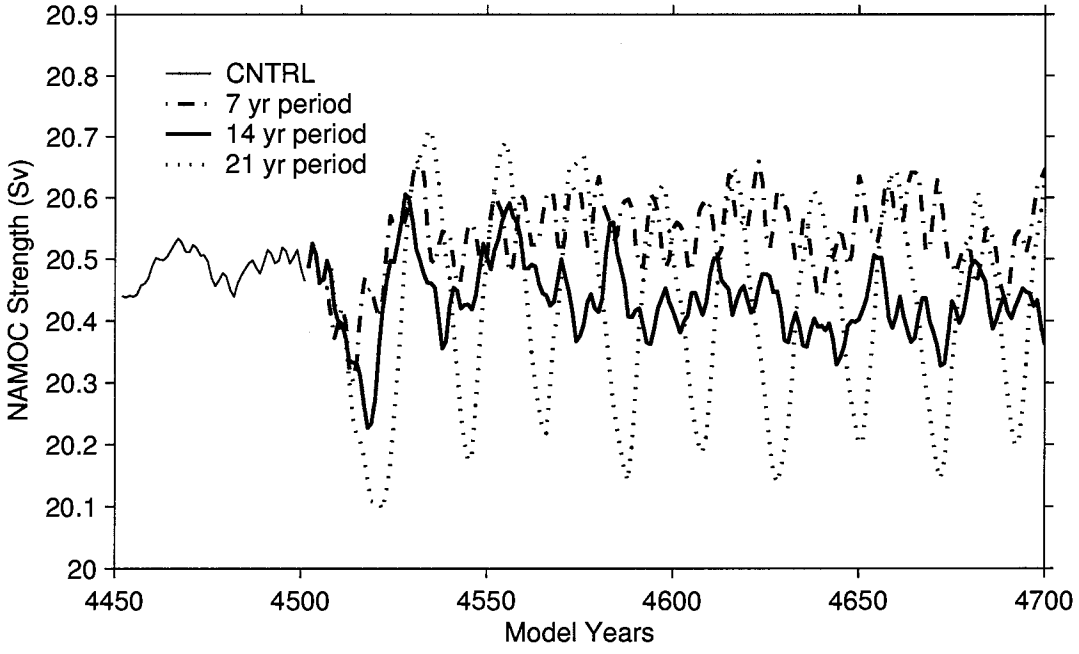

Figure 4.3: **The NAMOC response to sinusoidal tropical Atlantic freshwater forcings with a range of periods and distributed in the spatial pattern of Fig. 2.3b.**

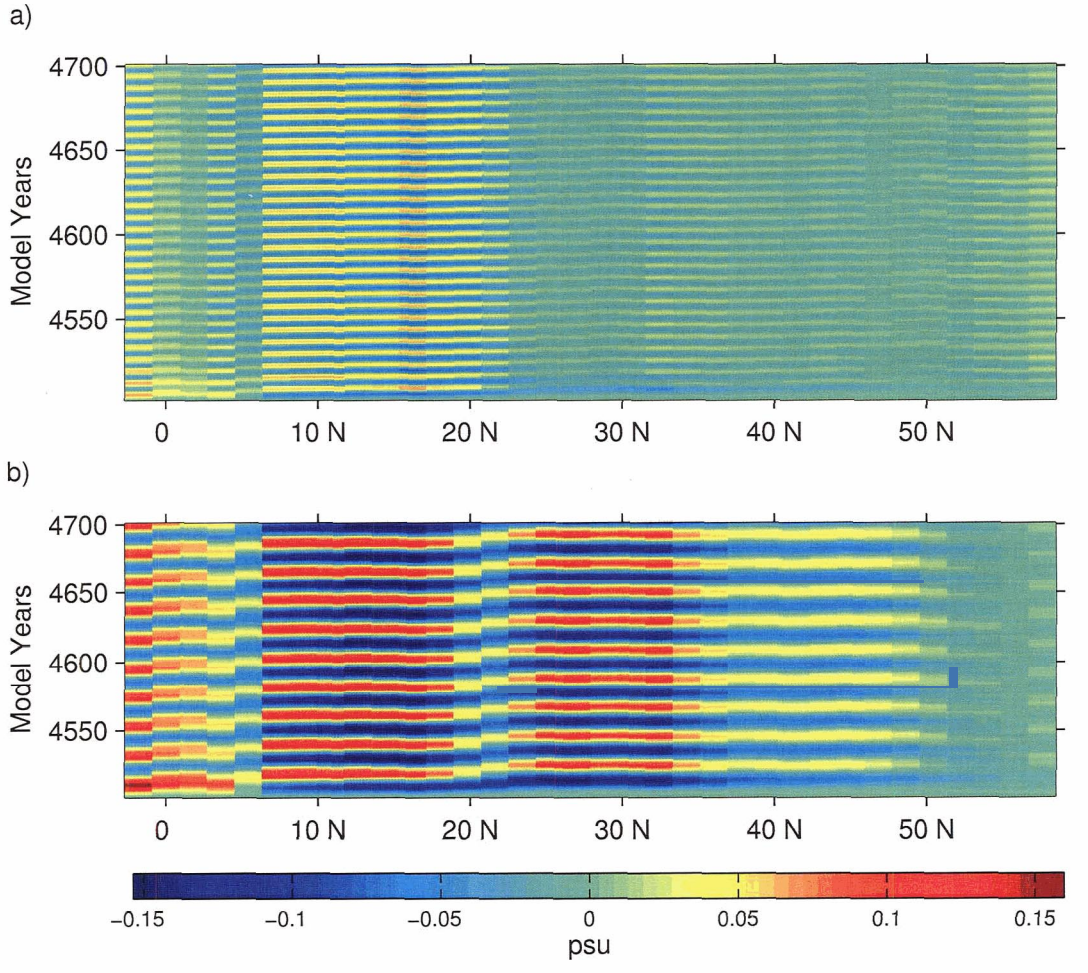

Figure 4.4: Hovmoeller diagrams showing the temporal evolution of near surface salinity anomalies as a function of latitude for the 7 year period (top frame (a)) and 21 year period (bottom frame (b)) forcings, respectively. Salinity anomalies are calculated from annually-averaged values as the difference from year 4500 of CNTRL, and then averaged both zonally and over the upper 356 m of the Atlantic Ocean. Freshwater forcings are distributed over the tropical Atlantic drainage basin in the spatial pattern of Fig. 2.3b. The annually-averaged salinity was recorded every year of the 200 year model runs.

I investigated the cause of this offset in another experiment wherein sinusoidal freshwater forcings were distributed evenly across the tropical Atlantic drainage basin. The amplitude of the new forcing signals was 1.5 Sv, which is equivalent to the 2 SD amplitude forcing discussed above. In this experiment the NAMOC response to the 7 year period forcing is no longer offset from the others and it disturbs the internal variability of the NAMOC to a lesser degree (Fig. 4.5). For the 14 year period forcing a weak quasi-sinusoidal NAMOC response is observed, with a frequency comparable to the forcing. I attribute the different NAMOC response in the previous experiment to the spatial variability in the satellite era NCEP50 regression (refer to Fig. 2.3b). In particular, the significant negative signal located around Lake Victoria, Africa, which discharges from the Congo river basin, adds an additional mode of variability to the sinusoidal forcings that complicates the NAMOC response. The signature of this negative signal is evident around the Equator in the Hovmoeller diagrams of Fig. 4.4, where the competing influences of discharges from the Congo and Amazon river basins mix.

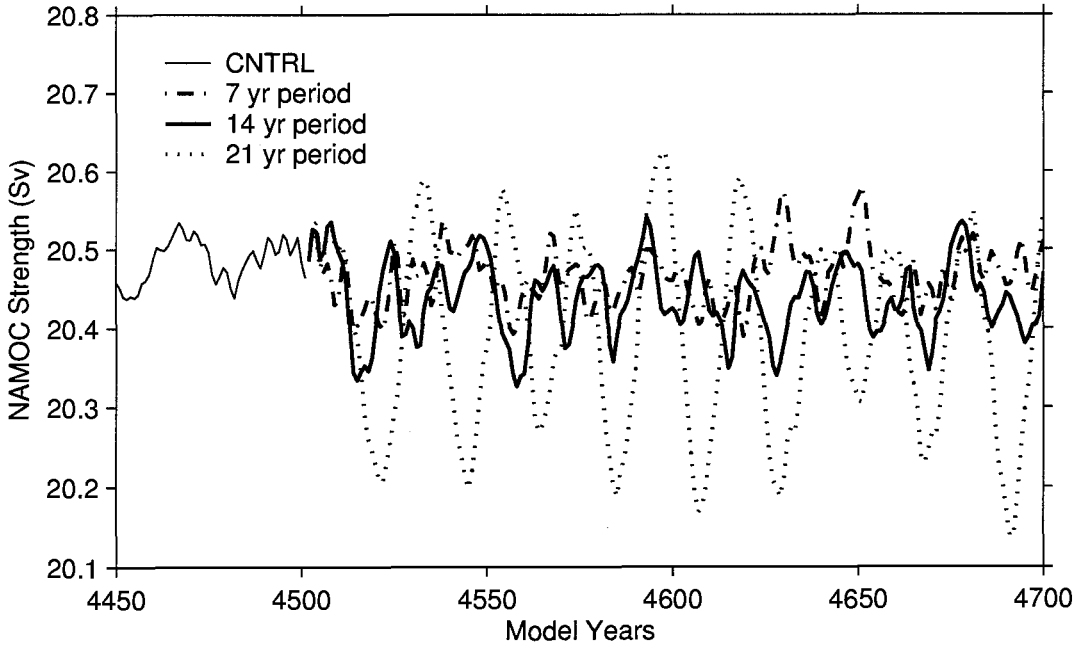

Figure 4.5: **Response of the NAMOC to sinusoidal tropical Atlantic freshwater forcings evenly distributed across the tropical Atlantic drainage basin between 20°N and 20°S. The amplitude of the forcing is 1.5 Sv.**

These results demonstrate the NAMOC to be sensitive to tropical Atlantic sinusoidal freshwater forcings with periods close to the advection timescale and longer. While NAMOC variability associated with freshwater forcings with the frequency and

amplitude of ENSO is not significant, decadal scale modulations of this freshwater forcing can have a weak impact on the NAMOC in the UVic ESCM (less than 0.5 Sv).

4.4 Response to NCEP50 Forcing

Here I examine the full influence of interannual tropical Atlantic surface freshwater variability on the NAMOC by applying NCEP50 P-E anomalies at each grid point within the tropical Atlantic basin of the UVic ESCM. To extend the forcing signal I simply cycle through the NCEP50 anomalies for a timespan of 200 years. This forcing signal is not limited to the influence of ENSO, but rather includes all modes of tropical Atlantic surface freshwater variability.

Figure 4.6 shows the response of the NAMOC when forced with the NCEP50 time series. There is a weak quasi-sinusoidal NAMOC response to the full-length NCEP50 forcing with a period, similar to the forcing period, that is amplified when the strength of the anomalies are doubled. The examination of the NCEP50 timeseries (Fig. 2.2) reveals the source of the decadal variability. Over the first 25 years of the NCEP50 times series, ending just prior to the start of the major La Niña event of 1973, the flux anomalies are largely negative, with a total of 7.4 $\times 10^6$ km^3 of freshwater exported from the basin. After 1973, a total of 9.3 $\times 10^6$ km^3 of freshwater is added to the basin. When the model is forced by anomalies cycled over these two time periods (also shown in Fig. 4.6) the persistent influence of these freshwater biases is observed. The NAMOC continues to strengthen when forced with anomalies cycled over the 1948/01 to 1972/12 period, and it continues to weaken when forced with anomalies cycled over the 1973/01 to 2004/12 period. These results indicate trends in the reanalysis to be the source of the modelled decadal NAMOC variability.

I now pose the question as to whether or not the decadal trends in the reanalysis are representative of real variability in tropical Atlantic freshwater fluxes. Kistler et al. (2001) point out that the correction of coding errors after 1972, along with the introduction of satellite data in 1979, added artificial 'jumps' to the reanalysis while improving its quality. This is why they strongly recommend calculating anomalies separately for the satellite era. When the ESCM is forced with NCEP50_SAT tropical Atlantic freshwater fluxes the steady state NAMOC variability is barely disturbed (Fig. 4.7). It is possible that the decadal NAMOC variability modelled under the full-length NCEP50 forcing is caused by changes in the quality of the reanalysis, rather than real variability in the tropical Atlantic freshwater balance.

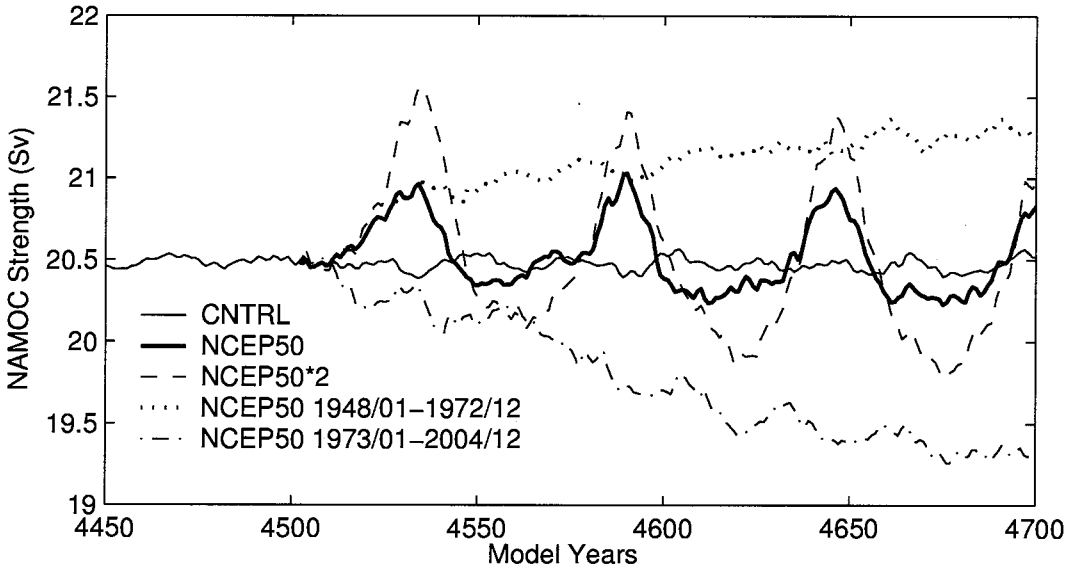

Figure 4.6: **Shown is the pre-industrial equilibrium CNTRL run NAMOC and its response to NCEP50 P-E anomalies applied at each grid point of the tropical Atlantic drainage basin and cycled for 200 years. Results are shown for the full-length NCEP50 anomalies (1948/01 to 200), the full-length anomalies multiplied by a factor of two, the first 25 years of the full-length anomalies, and the last 32 years.**

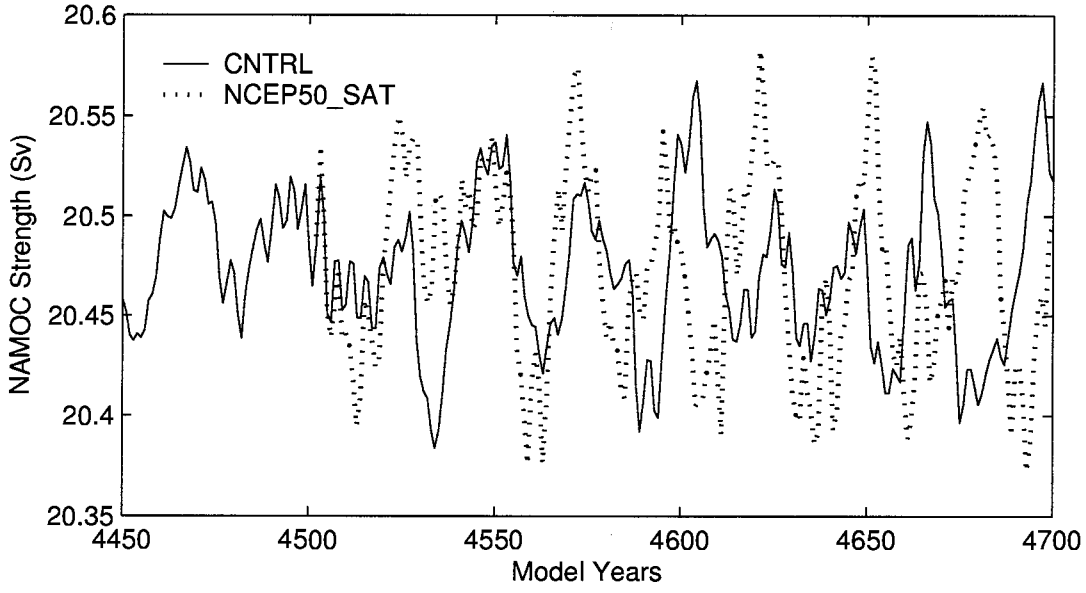

Figure 4.7: **Shown is the pre-industrial equilibrium CNTRL run NAMOC and its response to forcing from NCEP50_SAT anomalies (1979/01 to 2004/12). The forcing is applied at each grid point of the tropical Atlantic drainage basin and cycled for a period of 200 years.**

Chapter 5

NAMOC Response to Tropical Atlantic Freshwater Forcing with Increasing CO_2

5.1 Response to Increasing CO_2 and the Frequency of El Niño Events

I now examine the NAMOC response in the UVic ESCM to anthropogenic warming conditions with an increased frequency of El Niño related tropical Atlantic freshwater flux variability. The objective is to corroborate the results of Latif et al. (2000), which were produced by forcing the ECHAM4/OPYC model with an exponential increase of atmospheric CO_2 over 250 years according to the IS92A emission scenario. Latif et al. (2000) attributed an increased frequency of El Niño events in their model with the production of anomalously high tropical Atlantic salinity. They further argued that when the anomalous salinity was advected to the North Atlantic, it overwhelmed the anomalous freshwater input at high latitudes, resulting in a salinity increase in the range 0.5-0.7 psu when averaged over the upper 375m between 50°N and 55°N, and a stable NAMOC.

Figure 5.1 shows the NAMOC response in a UVic ESCM run, denoted WARM, wherein I follow the IS92A scenario and exponentially increase the atmospheric CO_2 from 280 ppm to 750 ppm over 250 years. The NAMOC in WARM weakens by 3.5 Sv, which places the UVic ESCM in the midrange of model responses published in the TAR (Houghton et al. 2001). A Hovmoeller diagram of salinity anomalies shows a decrease of 0.15 psu between 50°N and 55°N for the WARM model run (Fig. 5.2a).

Also included in Fig. 5.1 are the NAMOC responses to WARM forcing conditions applied simultaneously with the time series of tropical Atlantic freshwater forcings that simulate an increased frequency of El Niño events. Under WARM conditions with an equal split between El Niño and La Niña events, the NAMOC response is equivalent to that observed in WARM. Increasing the number of El Niño events

relative to La Niña events to 66%, 88% and 100% is found to mitigate the weakening of the NAMOC in WARM by only 14%, 23% and 36%, respectively. The Hovmoeller diagram of salinity anomalies from the 100% El Niño events run shows the advection of salinity from the tropics reduces the salinity decrease observed in WARM by 0.12 psu between 50°N and 55°N by the end of the run (Fig. 5.2b). Their remains a net decrease of 0.03 psu in the NADW formation region even when the tropical Atlantic is shifted to permanent El Niño conditions.

These results differ from those discussed in Latif et al. (2000). Significant increases in the frequency of El Niño related tropical Atlantic freshwater forcing does not substantially mitigate the reduction of the NAMOC in the UVic ESCM under anthropogenic warming conditions.

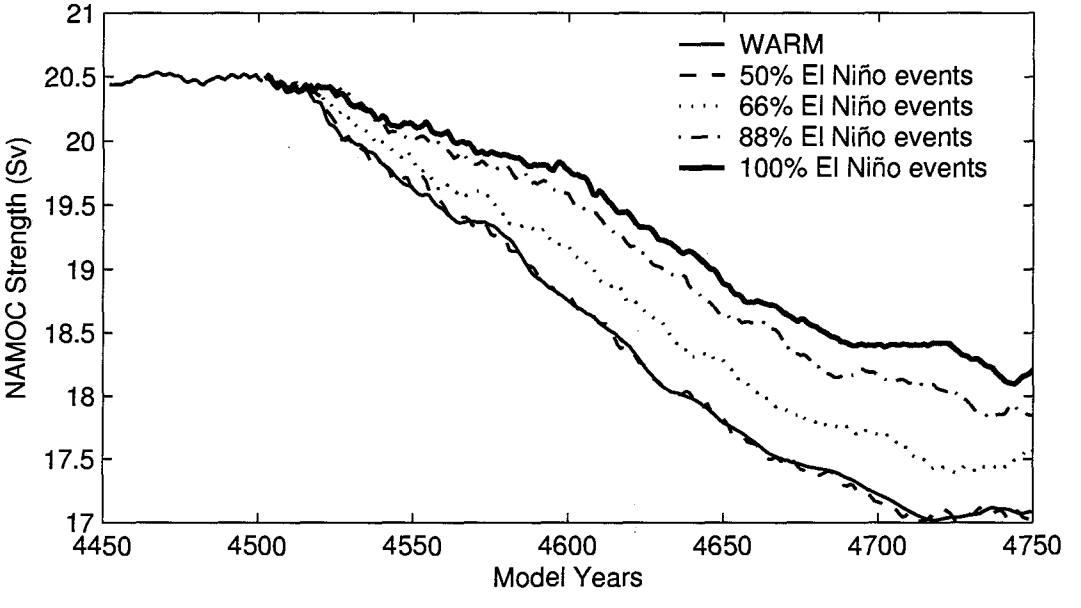

Figure 5.1: **Response of the NAMOC in the WARM model run, along with the NAMOC responses when the model is forced with the same CO_2 forcing as WARM and tropical Atlantic freshwater forcings that simulate different frequencies of El Niño events.**

5.2 Response to Increasing CO_2 and the Amplitude of El Niño Events

In this final sensitivity study I examine the impact on the NAMOC of increases in the amplitude of tropical Atlantic freshwater anomalies during El Niño events under anthropogenic warming conditions. There is an equal number of El Niño and La Niña

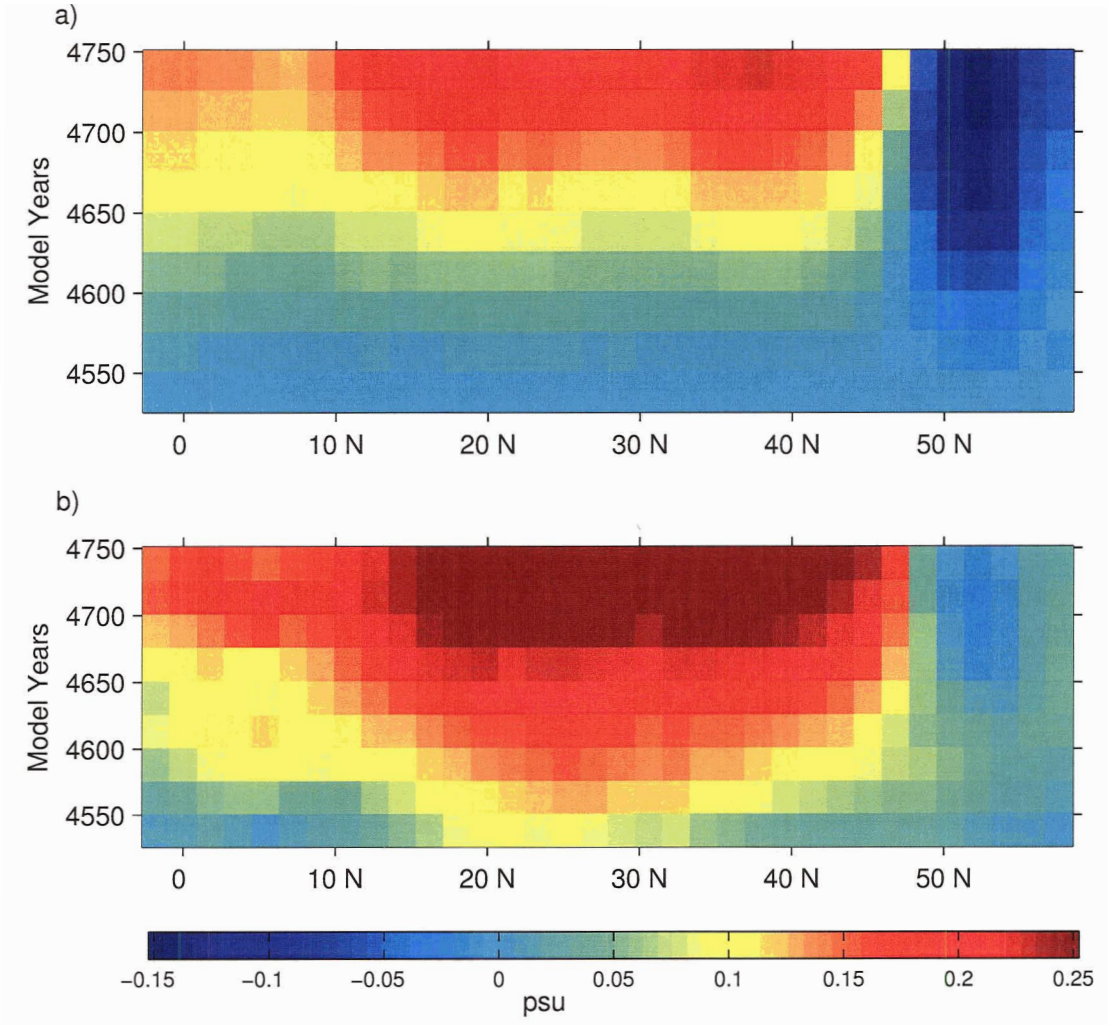

Figure 5.2: **Hovmoeller diagrams of the temporal evolution of near surface salinity anomalies as a function of latitude for the WARM model run (a), and the 100% El Niño events run (b). Salinity anomalies were calculated in the same manner as Fig. 4.4, except that annually-averaged salinity was recorded once every 25 years in these model runs.**

events in the freshwater forcing time series. Increasing the tropical Atlantic freshwater anomalies by 25% during El Niño events leads to a mitigation of only 7% of the weakening observed in the WARM run (Fig. 5.3). With a 50% and 100% increase in El Niño event anomalies the mitigation increases to 14% and 20%, respectively. The Hovmoeller diagram of ensemble average salinity anomalies from the 100% amplification run shows a reduction of the salinity decrease observed in WARM of 0.09 psu between 50°N and 55°N (Fig. 5.4).

Consistent with results presented in section 5.1, I find that significant increases in

the amplitude of El Niño related tropical Atlantic freshwater forcing does not substantially mitigate the reduction of the NAMOC in the UVic ESCM under anthropogenic warming conditions. In terms of the total freshwater forcing a 100% increase in amplitude is equivalent to increasing the frequency of El Niños to approximately 80%.

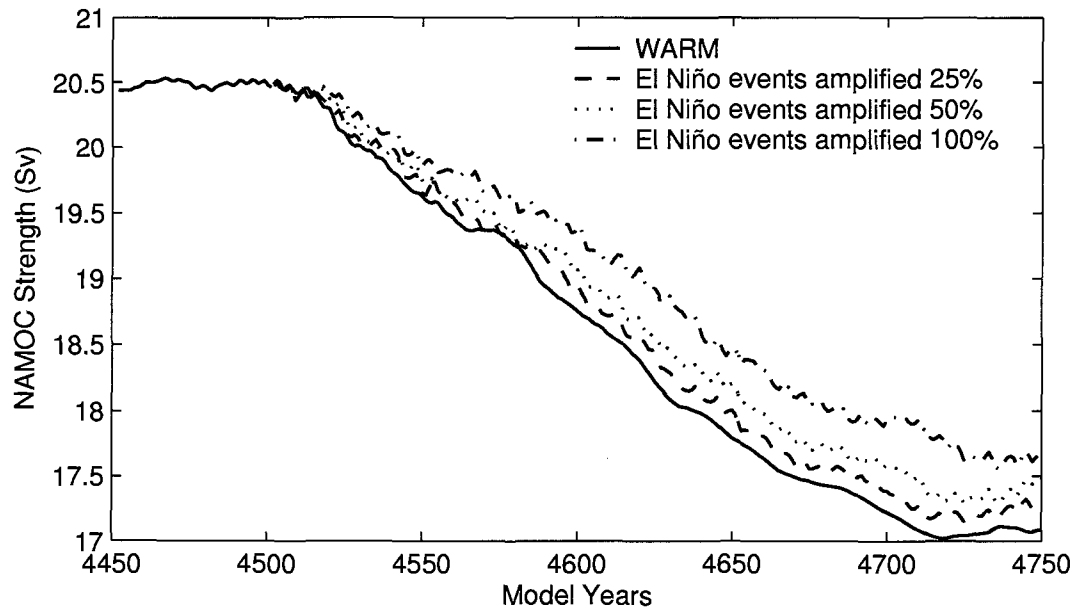

Figure 5.3: **Response of the NAMOC in the WARM model run, along with the NAMOC responses when the model is forced with the same CO_2 forcing as WARM and tropical Atlantic freshwater forcings that simulate increasing amplitudes of El Niño events.**

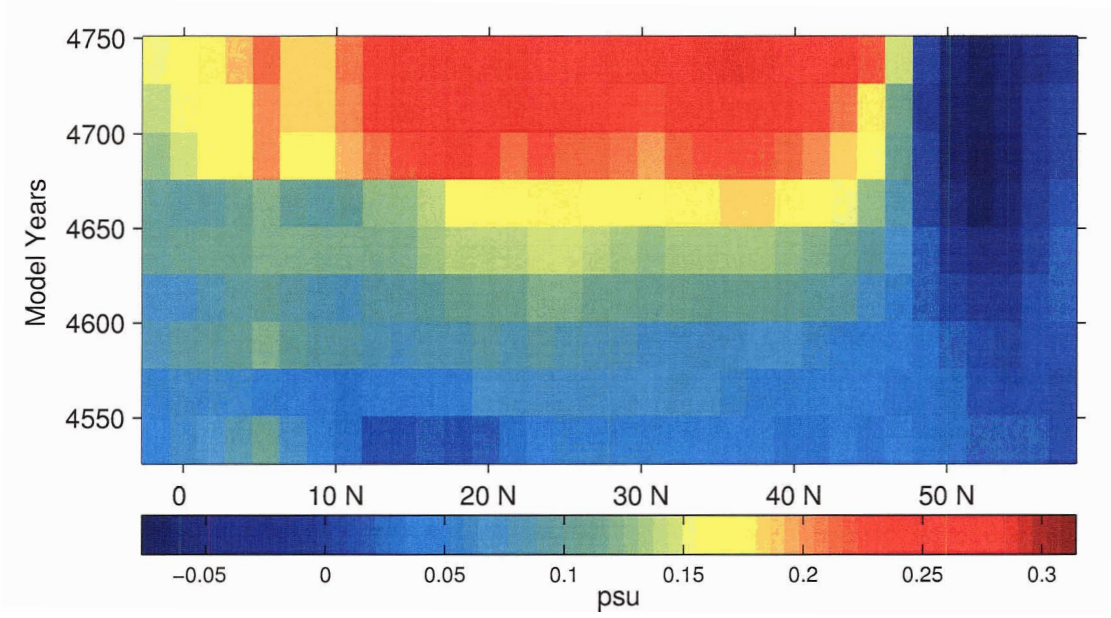

Figure 5.4: **Hovmoeller diagram of the temporal evolution of near surface salinity anomalies as a function of latitude for the 100% amplified El Niño events run. Salinity anomalies were calculated in the same manner as Fig. 4.4, except that annually-averaged salinity was recorded once every 25 years in this model run.**

Chapter 6

Conclusions

This study investigated interannual variability in tropical Atlantic surface freshwater flux and its impact on the NAMOC. I began by evaluating surface freshwater fluxes from ERA40 and NCEP50 reanalysis products, and the GPCP data set. The examination of ERA40 revealed unreasonable trends in tropical P that precluded its use in this study. Results from NCEP50 and GPCP support the strong correlation found by Schmittner et al. (2000) between ENSO and freshwater fluxes in the tropical Atlantic drainage basin. In a linear regression analysis I found that ENSO, represented by the SOI, accounted for roughly 55% of the interannual freshwater flux variability, with a one SD decrease in the SOI increasing the tropical Atlantic freshwater export by 0.09 Sv in NCEP50 and 0.1 Sv in GPCP.

I then used the UVic climate model to determine the impact of the northward propagation of tropical Atlantic salinity anomalies on the NAMOC equilibrated under pre-industrial levels of atmospheric CO_2. I found that tropical Atlantic salinity anomalies generated at the frequency and amplitude of ENSO-related variability do not impact deep water formation because they are diluted en route to the North Atlantic. However, decadal variability at the amplitude of ENSO does have a weak impact, with the rate of NADW formation increasing under El Niño conditions and decreasing under La Niña conditions by less than 5%.

Finally, I addressed the impact of an increased frequency of El Niño events under anthropogenic warming conditions on the NAMOC. Contrary to the results of Latif et al. (2000), I found that shifting the tropical Atlantic freshwater balance towards permanent El Niño conditions mitigates only 36% of the impact on deep water formation of warming and freshening at high latitudes. Similarly, I found that doubling the amplitude of El Niño events mitigates only 20% of the high latitude effects. Latif et al. (2000) explain their model results by noting that freshwater export in the tropical Atlantic increases by 0.3 Sv by the end of the integration. A comparison of this flux to NCEP50_SAT anomalies reveals that this is equivalent to shifting the tropical Atlantic freshwater balance to an El Niño state that is 2.5 times the magnitude of the 1998 event, which is one of the strongest on record. This magnitude of the ENSO response to warming is best put in context of an intercomparison of ENSO-like

variability in coupled climate models (Merryfield submitted). Under CO_2 doubling, three of the 15 models examined in the study exhibit statistically significant increases in ENSO amplitude, five exhibit significant decreases, and the ensemble average of the models presents a 5% fractional decrease in the period of ENSO.

Taken together, these results suggest that the poleward propagation of salinity anomalies from the tropical Atlantic should not be considered a significant mechanism for the variability of the NAMOC in the present and foreseeable future climate.

References

M.A. Alexander, I. Blade, M. Newman, J.R. Lanzante, N.C. Lau, and J.D. Scott. The atmospheric bridge: The influence of ENSO teleconnections on air-sea interaction over the global oceans. *Journal of Climate*, 15(16):2205–2231, 2002.

A. Baumgartner and E. Reichel. *The world water balance.* Elsevier Scientific Pub. Co, Germany, 1975.

C.M. Bitz, M.M. Holland, A.J. Weaver, and M. Eby. Simulating the ice-thickness distribution in a coupled climate model. *Journal of Geophysical Research*, 106(C2): 2441–2464, 2001.

G. Bond, W. Broecker, S. Johnsen, J. McManus, L. Labeyrie, J. Jouzel, and G. Bonani. Correlations between climate records from North Atlantic sediments and Greenland ice. *Nature*, 365(6442):143–147, 1993.

W. S. Broecker. Thermohaline circulation, the Achilles heel of our climate system: Will man-made CO_2 upset the current balance? *Science*, 278(5343):1583–1588, 1997.

K. Bryan and L. Lewis. Water mass model of the world ocean. *Journal of Geophysical Research*, 84(NC5):2503–2517, 1979.

G. Burgers. The El Niño stochastic oscillator. *Climate Dynamics*, 15(7):521–531, 1999.

L.S. Chiu, A.T. Chang, and J. Jonowiak. Comparison of monthly rain rates derived from GPI and SSM/I using probability distribution functions. *Journal of Applied Meteorology*, 32(2):323–334, 1993.

M. Cottet-Puinel, A.J. Weaver, C. Hillaire-Marcel, A. de Vernal, P.U. Clark, and M. Eby. Variation of Labrador Sea water formation over the last glacial cycle in a climate model of intermediate complexity. *Quaternary Science Reviews*, 23(3-4): 449–465, 2004.

D.L. Covey and S. Hastenrath. Pacific El Niño phenomenon and Atlantic circulation. *Monthly Weather Review*, 106(9):1280–1287, 1978.

S.C. Curtis and S. Hastenrath. Forcing of anomalous sea surface temperature evolution in the tropical Atlantic during Pacific warm events. *Journal of Geophysical Research*, 100(C8):15,835–15,847, 1995.

R.R. Dickson and J. Brown. The production of North Atlantic Deep Water: Sources, rates, and pathways. *Journal of Geophysical Research*, 99(C6):12,319–12,341, 1994.

W.J. Emery and R.E. Thomson. *Data Analysis Methods in Physical Oceanography.* Elsevier Scientific Pub. Co, New York, USA, 1998.

D.B. Enfield and D.A. Mayer. Tropical Atlantic sea surface temperature variability and its relation to El Niño Southern Oscillation. *Journal of Geophysical Research*, 102(C1):929–945, 1997.

A. Ganachaud and C. Wunsch. Improved estimates of global ocean circulation, heat transport and mixing from hydrographic data. *Nature*, 408(6811):453–457, 2000.

A. Ganachaud and C. Wunsch. Large-scale ocean heat and freshwater transports during the World Ocean Circulation Experiment. *Journal of Climate*, 16(4):696–705, 2003.

P.R. Gent and J.C. McWilliams. Isopycnal mixing in ocean circulation models. *Journal of Physical Oceanography*, 20(1):150 – 155, 1990.

A. Giannini, Y. Kushnir, and M.A. Cane. Interannual variability of Carribean rainfall, ENSO, and the Atlantic Ocean. *Journal of Climate*, 13(2):297–311, 2000.

A. Giannini, M.A.Cane, and Y. Kushnir. Interdecadal changes in the ENSO teleconnection to the Carribean region and the North Atlantic oscillation. *Journal of Climate*, 14(13):2867–2879, 2001.

J.K. Gibson, P. Kallberg, S. Uppala, A. Nomura, E. Serrano, and A. Hernandez. ERA description. ECMWF reanalysis project report 1: project organization. Technical report, European Centre for Medium Range Weather Forecast, Reading, http://www.ecmwf.int/publications/library/do/references/list/192, 1997.

M.C. Gregg. Scaling turbulent dissipation in the thermocline. *Journal of Geophysical Research*, 94(C7):9686 – 9698, 1989.

D.E. Harrison and N.K. Larkin. Darwin sea level pressure, 1876-1996: Evidence for climate change? *Geophysical Research Letters*, 24(14):1779–1782, 1997.

H. Hickey and A. J. Weaver. The Southern Ocean as a source region for tropical Atlantic variability. *Journal of Climate*, 17(20):3690–3972, 2004.

J.T. Houghton, Y. Ding, D.J. Griggs, M. Noguer, P.J. van der Lindend, X. Dai, K. Maskell, and C.A. Johnson, editors. *Climate Change 2001: The Scientific Basis.* Cambridge University Press, London, 2001.

G.J. Huffman, R.F. Adler, P. Arkin, A. Chang, R. Ferraro, A. Gruber, J. Janowiak, A. McNab, B. Rudolf, and U. Schneider. The Global Precipitation Climatology Project (GPCP) combined precipitation dataset. *Bulletin of the American Meteorological Society*, 78(1):5–20, 1997.

E. C. Hunke and J. K. Dukowicz. An elastic-viscous-plastic model for sea ice dynamics. *Journal of Physical Oceanography*, 27:1849–1867, 1997.

S. Janicot, S. Trzaska, and I. Poccard. Summer Sahel-ENSO teleconnection and decadal time scale SST variations. *Climate Dynamics*, 18(3/4):303–320, 2001.

J.E. Janowiak, A. Gruber, C.R. Kondragunta, R.E. Livezey, and G.J. Huffman. A comparison of the NCEP-NCAR reanalysis precipitation and the GPCP rain gauge-satellite combined dataset with observational error considerations. *Journal of Climate*, 11(11):2960–2979, 1998.

F.F. Jin, J.D. Neelin, and M. Ghil. El Niño on the Devils staircase - annual subharmonic steps to chaos. *Science*, 264(5155):70–72, 1994.

P. Kållberg, A. Simmons, S. Uppala, and M. Fuentes. Era-40 project report series no. 17: The ERA-40 archive. Technical report, European Centre for Medium Range Weather Forecast, Reading, http://www.ecmwf.int/publications/library/do/references/list/192, 2004.

E. Kalnay, M. Kanamitsu, R. Kistler, W. Collins, D. Deaven, L. Gandin, M. Iredell, S. Saha, G. White, J. Woollen, Y. Zhu, A. Leetmaa, R. Reynolds, M. Chelliah, W. Ebisuzaki, W. Higgins, J. Janowiak, K.C. Mo, C. Ropelewski, J. Wang, R. Jenne, and D. Joseph. The NCEP/NCAR 40-year reanalysis project. *Bulletin of American Meteorological Society*, 77(3):437 – 471, 1996.

R. Kistler, E. Kalnay, W. Collins, S. Saha, G. White, J. Woollen, M. Chelliah, W. Ebisuzaki, M. Kanamitsu, V. Kousky abd H. van den Dool, R. Jenne, and M. Fiorino. The NCEP-NCAR 50-year reanalysis: Monthly means CD-ROM and

documentation. *Bulletin of the American Meteorological Society*, 82(2):247–267, 2001.

T.T. Knutson and S. Manabe. Model assessment of decadal variability and trends in the tropical Pacific Ocean. *Journal of Climate*, 11(9):2273–2296, 1998.

M. Latif, E. Roeckner, U. Mikolajewicz, and R. Voss. Tropical stabilization of the thermohaline circulation in a greenhouse warming simulation. *Journal of Climate*, 13(11):1809–1813, 2000.

N.C. Lau and M.J. Nath. A modelling study of the relative roles of tropical and extratropical SST anomalies in the variability of the global atmosphere-ocean system. *Journal of Climate*, 7(8):1184–1207, 1994.

J.P. Lewis, A.J. Weaver, S.T. Johnston, and M. Eby. Neoproterozoic "snowball Earth": Dynamic sea ice over a quiescent ocean. *Paleoceanography*, 18(4):16(1)–16(8), 2003.

S. Manabe and R. J. Stouffer. Two stable equilibria of a coupled ocean atmosphere model. *Journal of Climate*, 1:841–866, 1988.

J. Marshall and F. Schott. Open-ocean convection: Observations, theory and models. *Reviews of Geophysics*, 37(1):1–64, 1999.

H.D. Matthews, A.J. Weaver, M. Eby, and K.J. Meissner. Radiative forcing of climate by historical land cover change. *Geophysical Research Letters*, 30(2):27(1)–27(4), 2003.

K. J. Meissner, A. Schmittner, A. J. Weaver, and J. F. Adkins. Ventilation of the North Atlantic Ocean during the Last Glacial Maximum: A comparison between simulated and observed radiocarbon ages. *Paleoceanography*, 18(2):1023, 2003.

W.J. Merryfield. Changes to ENSO under CO_2 doubling in the IPCC AR4 coupled climate models. *Journal of Climate*, submitted.

J.D. Neelin, D.S. Battisti, A.C. Hirst, F. Jin, Y Wakata, T. Yamagata, and S.E. Zebiak. ENSO theory. *Journal of Geophysical Research*, 103(C7):14261–14290, 1998.

NOAA. National Oceanic and Atmospheric Association Climate Prediction Center monthly atmospheric and sea surface temperature indices, 2005a. URL `http://www.cpc.ncep.noaa.gov/data/indices/`.

NOAA. National Oceanic and Atmospheric Association Climate Prediction Center monthly atmospheric and sea surface temperature indices: How is the SOI calculated?, 2005b. URL `http://www.cpc.ncep.noaa.gov/data/indices/Readme.index.shtml`.

A. Oka and H. Hasumi. Effects of freshwater forcing on the Atlantic deep circulation: A study with an OGCM forced by two different surface freshwater flux datasets. *Journal of Climate*, 17(11):2180–2194, 2004.

R. Pacanowski. *MOM 2 Documentation User's Guide and Reference Manual, GFDL Ocean Group Technical Report.* NOAA/GFDL, Princeton, 1995.

K.L. Polzin, J.M. Toole, and R.W. Schmitt. Finescale parameterizations of turbulent dissipation. *Journal of Physical Oceanography*, 25(2):306–328, 1995.

V.B. Rao, M.C. De Lima, and S.H. Franchito. Seasonal and interannual variations of rainfall over northeast Brazil. *Journal of Climate*, 6(9):1754–1763, 1993.

C.F. Ropelewski and M.S. Halpert. Global and regional scale precipitation patterns associated with the El Niño Southern Oscillation. *Monthly Weather Review*, 115 (8):1606–1626, 1987.

R. Saravanan and P. Chang. Interaction between tropical Atlantic variability and El Niño Southern Oscillation. *Journal of Climate*, 13(13):2177–2194, 2000.

A. Schmittner, C. Appenzeller, and T. F. Stocker. Enhanced Atlantic freshwater export during El Niño. *Geophysical Research Letters*, 27(8):1163–1166, 2000.

A. Schmittner, K. J. Meissner, M. Eby, and A. J. Weaver. Forcing of the deep ocean circulation in simulations of the Last Glacial Maximum. *Paleoceanography*, 17(2): 1015, 2002.

H. Stommel. Thermohaline convection with two stable regimes of flow. *Tellus*, 13: 224–230, 1961.

L.D. Talley, J.L. Reid, and P.E. Robbins. Data-based meridional overturning streamfunctions for the global ocean. *Journal of Climate*, 16(19):3213–3226, 2003.

A. Timmermann, J. Oberhuber, A. Bacher, M. Esch, M. Latif, and E. Roeckner. Increased El Niño frequency in a climate model forced by future greenhouse warming. *Nature*, 398(6729):694–697, 1999.

K. E. Trenberth and T.J. Hoar. The 1990-1995 El Niño Southern Oscillation event: Longest on record. *Geophysical Research Letters*, 23(1):57–60, 1996.

A. Troccoli and P. Kallberg. ERA-40 project report series no. 13: Precipitation correction in the ERA-40 reanalysis. Technical report, European Centre for Medium Range Weather Forecast, Reading, http://www.ecmwf.int/publications/library/do/references/list/192, 2004.

E. Tziperman, L. Stone, M.A. Cane, and H.Jarosh. El Niño chaos - overlapping of resonances between the seasonal cycle and the Pacific Ocean-Atmosphere Oscillator. *Science*, 264(5155):72–74, 1994.

J.M. Wallace, E.M. Rasmusson, T.P. Mitchell, V.E. Kousky, E.S. Sarachik, and H. von Storch. On the structure and evolution of ENSO-related climate variability in the tropical Pacific: Lessons from TOGA. *Journal of Geophysical Research*, 103(C4): 14241–14259, 1998.

A. J. Weaver. The UVic Earth System Climate Model and the thermohaline circulation in past, present and future climates. *The State of the Planet: Frontiers and Challenges in Geophysics, IUGG and AGU Geophysical Monograph Series*, 150: 279–296, 2004.

A. J. Weaver, M. Eby, E. C. Wiebe, C. M. Bitz, P. B. Duffy, T. L. Ewen, A. F. Fanning, M. M. Holland, A. MacFadyen, H. D. Matthews, K. J. Meissner, O. Saenko, A. Schmittner, H. X. Wang, and M. Yoshimori. The UVic Earth System Climate Model: Model description, climatology, and applications to past, present and future climates. *Atmosphere-Ocean*, 39(4):361–428, 2001.

A. J. Weaver and T. M. Hughes. Stability and variability of the thermohaline circulation and its link to climate. *Trends in Physical Oceanography, Research Trends Series, Council of Scientific Research Integration, Trivandrum, India*, 1(1):15–70, 1992.

E.C. Wiebe and A.J. Weaver. On the sensitivity of global warming experiments to the parameterization of sub-grid scale ocean mixing. *Climate Dynamics*, 15(12): 875–893, 1999.

C. Wunsch. The interpretation of short climate records, with comments on the North Atlantic and Southern Oscillations. *Bulletin of the American Meteorological Society*, 80(2):245–255, 1999.

J.M. Yoo and J.A. Carton. Annual and interannual variation of the freshwater budget in the tropical Atlantic Ocean and the Carribean Sea. *Journal of Physical Oceanography*, 20:831–845, 1990.

Appendix A

The Sliding 12 Month Low Pass Filter

This appendix describes the routine used to filter fluctuations of period less than a year from one dimensional time series of monthly data. The filter applies a sliding window composed of the 13 data points, of which six precede and six follow the centre value. The centre value in the window is replaced with the average value of all the points. When the sliding window exceeds the lower or upper boundaries of the input series, the average is computed among the available points. The following is a sample of the functioning of the filter routine:

$$Input = [1 \quad 3 \quad -8 \quad 5 \quad 1 \quad 2 \quad -4 \quad -3 \quad -1 \quad 6 \quad 2 \quad 8 \quad 9], \tag{A.1}$$

$$\begin{aligned} Output = [0 \quad -0.38 \quad -0.44 \quad 0.20 \quad 0.36 \quad 1.00 \quad 1.62 \quad ... \\ 1.67 \quad 1.54 \quad 2.50 \quad 2.22 \quad 2.38 \quad 2.42]. \end{aligned} \tag{A.2}$$

Appendix B

Linear Least Squares Regression

This appendix illustrates the linear regression algorithm used in this dissertation. Emery and Thomson (1998) provides a more complete discussion. A linear regression determines the linear relationship between a dependent times series, y_i, (e.g. fresh-water fluxes) and an independent regressor time series, x_i, (e.g. the SOI). The least squares fit of y_i on x_i is done by solving the linear model

$$y_i = \hat{y}_i + \epsilon_i \tag{B.1}$$

where

$$\hat{y}_i = b_0 + b_1 x_i \tag{B.2}$$

is the estimator for the deterministic portion of the data and ϵ is the error (or residual). To find the best regression coefficients, b_0 and b_1, the error is minimized in a least squares sense. This is done by calculating the variance in the data, or the sum of the squares total (SST), as

$$SST = \sum_{i=1}^{N} (y_i - \bar{y}_i)^2 \tag{B.3}$$

and the the variance explained by the regression model, or sum the of the squares regression (SSR), as

$$SSR = \sum_{i=1}^{N} (\hat{y}_i - \bar{y}_i)^2. \tag{B.4}$$

The total variance that is not accounted for by the regression model (SSE) is then calculated as

$$SSE = SST - SSR = \sum_{i=1}^{N} [y_i - (b_0 + b_1 x_i)]^2. \tag{B.5}$$

The unexplained variance in the regression is then minimized by setting

$$\frac{\partial SSE}{\partial b_0} = 0 \tag{B.6}$$

and

$$\frac{\partial SSE}{\partial b_1} = 0. \tag{B.7}$$

These equations can then be solved simultaneously to find an estimate of b_1 (the slope of the regression line), which is then used to obtain an estimate of b_0 (the intercept of the regression line). In particular,

$$\hat{b}_1 = \frac{\sum_{i=1}^{N}(x_i - \bar{x})(y_i - \bar{y})}{\sum_{i=1}^{N}(x_i - \bar{x})^2} \tag{B.8}$$

and

$$\hat{b}_0 = \bar{y} - \hat{b}_1 \bar{x}. \tag{B.9}$$

The ratio of SSR/SST (variance explained/total variance) is a measure of the quality of the regression fitting (or correlation of determination) and is commonly denoted as r^2. For a perfect regression fit SSE = 0 and $r^2 = 1$. The correlation coefficient, r, is a measure of how well two variables vary in time. The magnitude of r is easily solved by taking $\sqrt{SSR/SST}$ and the actual value of r can be solved for as

$$r = \frac{1}{N-1}\frac{\sum_{i=1}^{N}(x_i - \bar{x})(y_i - \bar{y})}{SD_x SD_y} \tag{B.10}$$

where SD (standard deviation) is solved as

$$SD_x = \sqrt{\frac{1}{N-1}\sum_{i=1}^{N}(x_i - \bar{x})^2}. \tag{B.11}$$

It is important to note that a high correlation between x and y does not imply causation or that x will be a good predictor of y in the future. The determination of confidence intervals for r and b_1 are done by calculating the standard error of the estimate, s_e, as

$$s_e = [\frac{SSE}{N-2}]^{1/2} \tag{B.12}$$

and assuming that s_e is from a Gaussian distribution with a mean of 0. In this case 95% of the observations will fall within $\pm 2s_e$ of the regression line.